This is a preprint, the final version is subject to change, of the American Mineralogist (MSA)
Cite as Authors (Year) Title. American Mineralogist, in press.
DOI: https://doi.org/10.2138/am-2020-7062

Revision 1

Formation of native arsenic in hydrothermal base metal deposits and related supergene U^{6+}- enrichment: the Michael vein near Lahr, SW Germany

Manuel Scharrer[1], Katharina Sandritter[1], Benjamin F. Walter[1,2], Udo Neumann[1] & Gregor Markl[1]

[1] Department of Geoscience, University of Tuebingen, Wilhelmstr. 56, D-72074 Tübingen

[2] Present address: Institute for Applied Geoscience, Karlsruhe Institute of Technology (KIT), Adenauerring 20b, D-76313 Karlsruhe

Corresponding author: Manuel Scharrer

Email addresses:

Manuel Scharrer: manuel.scharrer@uni-tuebingen.de

Katharina Sandritter: Katharina_Sandritter@gmx.de

Benjamin F. Walter: benjamin.walter@uni-tuebingen.de

Udo Neumann: udo.neumann@uni-tuebingen.de

Gregor Markl: markl@uni-tuebingen.de

Abstract

Native arsenic is an occasional ore mineral in some hydrothermal base metal deposits. Its rarity (compared to pyrite, arsenopyrite, galena, sphalerite or chalcopyrite, for example) is surprising, as arsenic is a common constituent of upper crustal fluids. Hence, the conditions of formation must be quite special to precipitate native arsenic. An ideal location to investigate the formation of native As and to explore the parameters constraining its crystallization is the Michael vein near Lahr, Schwarzwald, SW Germany. Here, galena, sphalerite and native arsenic are the most abundant ore minerals. The two important ore stages comprise 1. galena-barite and 2. sphalerite-native arsenic-quartz, the latter with a general mineral succession of pyrite → sphalerite ± jordanite-gratonite solid solution → galena → native As. The native arsenic-bearing mineralization formed by cooling of at least 130 °C hot saline fluid accompanied by reduction due to admixing of a sulfide-bearing fluid.

Thermodynamic calculations reveal that for the formation of native arsenic, reduced conditions in combination with very low concentrations of the transition metals Fe, Co, and Ni, as well as low sulfide concentrations, are essential. "Typical" hydrothermal fluids do not fulfill these criteria, as they typically can contain significant amounts of Fe and sulfide. This results in the formation of arsenides, sulfarsenides, or As-bearing sulfides instead of native arsenic. Very minor amounts of pyrite, sulfarsenides and arsenides record the very low concentrations of Fe, Co and Ni present in the ore-forming fluid. High concentrations of aqueous Zn and Pb lead to early saturation of sphalerite and galena which promoted native arsenic precipitation by decreasing the availability of sulfide and hence suppressing realgar formation.

Interestingly, native arsenic in the Michael vein acted as a trap for uranium during supergene weathering processes. Infiltrating oxidizing, U^{+VI}-bearing fluids from the host lithologies reacted

under ambient conditions with galena and native arsenic forming a variety of U^{+VI} (±Pb)-bearing arsenates such as hügelite, hallimondite, zeunerite, heinrichite or novacekite together with U-free minerals like mimetite or anglesite. Some parts of the vein were enriched to U concentrations of up to 1 wt% by this supergene process. Reduced (hypogene) uranium phases like uraninite were never observed.

Keywords:

- native arsenic
- jordanite-gratonite
- hydrothermal
- base metal
- uranylarsenates
- hallimondite

Introduction

Although arsenic is not a rare element in soils and upper crustal waters (e.g., Dudas, 1987; Nordstrom, 2002; Peters et al., 2006; Drahota and Filippi, 2009), native arsenic is a relatively rare mineral (< 400 localities worldwide reported in mindat.org in March 2019). However, in some types of ore deposits, it occurs in large quantities and samples up to dozens of kilograms have been recovered (e.g., Hösel, 2003; Ondrus et al., 2003; Hiller and Schuppan, 2008). Arsenic is a toxic metalloid, and some of its compounds are harmful to the environment and human health (e.g., Bowell et al., 2014; Mitchell, 2014). Therefore, numerous recent publications have studied the abundance, sorption behavior, biotic and abiotic mobility, and redistribution of arsenic at ambient conditions (e.g., Pierce and Moore, 1982; Nordstrom and Young, 2000; Mandal and Suzuki, 2002; Nordstrom, 2002; Drahota and Filippi, 2009; Amend et al., 2014; Bowell et al., 2014; Bowell and Craw, 2014; Mitchell, 2014; Wu et al., 2017). However, at higher temperature, the behavior of arsenic is considerably less investigated and understood, although arsenic is a common element in various hydrothermal systems (e.g., Ballantyne and Moore, 1988; Horton et al., 2001; Price and Pichler, 2005).

Arsenic naturally occurs in six oxidation states (As^{-II}, As^{-I}, As^{0}, As^{+II}, As^{+III} and As^{+V}), and forms a variety of gaseous, aqueous, and solid species of different toxicity (e.g., Boitsov and Kaikova, 1965; Sergeyeva and Khodakovskiy, 1969; Pokrovski et al., 2013; Keller et al., 2014; Nordstrom et al., 2014). Thus, redox state and redox reactions play a crucial role in processes involving arsenic. Dissolved arsenic is present as As^{+V} under oxidized and/or basic conditions, and as As^{+III} under more reducing and/or neutral to acidic conditions, occurring as ions or complexes. Under geothermal conditions, As^{+III}, in the form of $As(OH)_3$, is the most common species of dissolved As (e.g., Sergeyeva and Khodakovskiy, 1969; Ballantyne and Moore, 1988; Criaud and Fouillac,

1989; Zheng et al., 2015). The formation of oxide and hydroxide complexes (mainly arsenate and arsenite) leads to a high solubility of arsenic (e.g., Glaskova et al., 1999). This solubility is, however, greatly decreased due to enhanced mineral precipitation in the presence of transition metals such as Ni, Co, Fe, and/or under reduced conditions (e.g., Glaskova et al., 1999; Markl et al., 2016; Kreissl, 2018). In turn, this implies that the presence and redox state of arsenic is essential in defining the mobility of other elements, and thus the formation of specific minerals both in hydrothermal and near-surface processes. The source of arsenic in a specific enrichment zone (i. e., deposit, placer, weathering crust...) can be highly variable, since groundwater, metamorphic fluids, magmatic fluids, as well as brines have been proposed to form arsenic-rich mineralizations (e.g., Robinson and Ohmoto, 1973; Migdisov and Bychkov, 1998; Essarraj et al., 2005; Su et al., 2009; Epp et al., 2018). The aim of the present study is to investigate the fate of arsenic in hydrothermal base-metal vein-type deposits, the relative importance of dissolved species, and the stable As-phases formed during mineral precipitation rather than the origin of the As-bearing fluid.

Specifically, the present contribution will focus on the natural occurrence of native arsenic (nat. As). Where present, it generally forms as an abundant hypogene mineral under hydrothermal conditions (e.g., Vokes, 1963; Nokleberg, 2005; Voudouris et al., 2008; Radosavljević et al., 2014; Zheng et al., 2015; Burisch et al., 2017a) or as a minor mineral during the breakdown of As-bearing minerals/solid solutions (Cook, 1996). It is common in five-element associations (Reuss, 1863; Hiller and Schuppan, 2008; Pekov et al., 2010; Staude et al., 2012; Burisch et al., 2017a), much less common, though, in "normal" base-metal-rich veins with galena, sphalerite, and/or chalcopyrite. Mineralization types with nat. As are assembled in Table 1.

A mineralogically particularly interesting example of a native arsenic-bearing base-metal vein is the Michael mine near Lahr, Schwarzwald, SW Germany, since it operated on a hydrothermal vein comprised of a simple base metal mineralogy (galena, barite), followed by a hydrothermal phase of quartz with native arsenic and base-metal sulfides (galena, sphalerite) and a supergene enrichment of uranium by the formation of uranyl arsenates. Based on numerous studies on the geology, mineralogy, geochemistry, and conditions of formation of Schwarzwald hydrothermal veins (e.g., Burisch et al., 2016; Walter et al., 2017; Walter et al., 2018), this occurrence provides an ideal case to study the fate of arsenic in a Pb-Zn-base metal hydrothermal environment. A specific focus will be put on the conditions of formation of nat. As, in comparison to the more common arsenic-bearing hydrothermal minerals such as sulfarsenides and As-bearing sulfosalts/sulfides.

Regional geology and geochemical background

The Michael mine is situated in the central Schwarzwald near Lahr and on the eastern flank of the Upper-Rhine-Graben (Fig. 1). Its radioactivity led to a detailed investigation in the 1950's, during the search for uranium in Western Europe. During this time, samples were taken underground and mineralogically investigated by Walenta and Wimmenauer (1961) and by Kirchheimer (1957), without finding an economic uranium mineralization. The local geology consists of a Variscan crystalline basement discordantly overlain by a terrestrial to marine sedimentary cover, which are both tectonically uplifted and overprinted by a normal fault-dominated regime due to the opening of the Upper Rhine Graben (URG) during the Paleogene. An inclined uplift of the rift flanks led to partial erosion of the Paleozoic and Mesozoic sedimentary cover sequence resulting in the present day topography (Geyer et al., 2011 and references therein).

The Michael vein is at least 1.3 km long and up to 2 meters wide (average of 80 cm; Bliedtner and Martin, 1986). It is hosted by crystalline basement consisting of late Variscan post-collisional granites and cordierite- and graphite-bearing metasedimentary gneisses and metatexites (Kirchheimer, 1957; Metz and Richter, 1957; Walenta and Wimmenauer, 1961; Kaiser, 1983). It occurs on a rift-parallel normal fault that juxtaposes Rotliegend rhyolitic volcanics and clastic sediments, Buntsandstein and crystalline basement (Fig. 1; Geyer et al., 2011). The sedimentary units overlaying the Buntsandstein are abundant to the east, at the far side of the rift flank, and inside the graben structure, but due to long-lasting erosion and rift flank uplift, they are no longer present in the area of investigation (Geyer et al., 2011). Paleogene sediments of up to 4000 m thickness occur in the URG, including Oligocene halite-bearing evaporites (Geyer et al., 2011).

The URG rifting as well as previous large scale tectonic events have resulted in five hydrothermal maxima (Pfaff et al., 2009; Staude et al., 2012; Walter et al., 2016) producing more than 1000 mineralized hydrothermal veins in the Schwarzwald mining district between Karlsruhe and Basel. These veins consist dominantly of barite, fluorite, quartz, and carbonates besides base and precious metal oxides, sulfides, and arsenides (Metz and Richter, 1957; Bliedtner and Martin, 1986; Staude et al., 2009). The last hydrothermal maximum (post-Cretaceous) was related to the URG rifting; juxtaposition of different rock units in conjunction with abundant small- to large-scale fracturing led to the connection of different fluid aquifers which were separated prior to this tectonic activity (Walter et al., 2018). This favored a multi-fluid mixing scenario which resulted in the formation of mineralogically diverse hydrothermal veins (Walter et al., 2018).

Sample location

Samples analyzed in this study were taken from the dumps of the Michael vein, from the mineralogical collection of the University of Tübingen and the Geological Survey of Baden-Württemberg (among them samples from the most comprehensive study of this vein by Kirchheimer 1957), and from the private collection of the last author. The samples cover the whole mineralogical diversity of the vein and originate from both mine dumps and (the Kirchheimer samples) from underground. The Michael vein was worked from two historic adits; the Michael mine at the southern end of the vein and the Silbereckle mine close to its northern end (Fig. 1). Samples from both mines and from dumps in between were investigated.

Petrography of the mineralization

Based on detailed ore microscopy and macroscopic observations in addition to observations from the literature, the mineralization consists of three hydrothermal stages, with more than 95 vol.% of the mineralization formed during the first two stages (Fig. 2). An initial, barite- and galena-dominated stage (Fig. 3a) was followed by the formation of a quartz-sphalerite-native arsenic assemblage (Fig. 3b-d), which in turn was overgrown by small amounts of carbonates (calcite, dolomite). Supergene processes resulted in the formation of typical secondary Pb and Zn phases and, interestingly, in the formation of uranium minerals, although primary (=hypogene) uranium phases are missing.

The vein itself is characterized by intense tectonic brecciation, partial dissolution of earlier and subsequent cementation by successive minerals. Thus, the relative ages of individual minerals have been interpreted not based on individual, but on the sum of all available textures. Interestingly, there is a gradual transition in the manifestation of the second ore stage from north

174 to south, with a more colloform and skeletal appearance in the north (Fig. 3c) and well-
175 crystallized minerals in the south (Fig. 3d). The mineralogical differences between these textural
176 variations of stage 2 mineralization are shown in Fig. 2b.

177

178 I. Barite stage: Quartz is the initial mineral of stage I and forms as a rim on host rock fragments.
179 It is directly overgrown by abundant barite forming white to slightly yellow fans of slender
180 needle crystals occasionally arranged in an unusual cauliflower-like texture (Fig. 3a). The inter-
181 crystal porosity of the barite crystals is commonly filled by quartz which intermediately forms
182 during barite crystallization (Walenta and Wimmenauer, 1961; Krahé, 2012). The only ore of
183 this barite stage consists of up to several centimeters large euhedral galena crystals embedded in
184 barite (Fig. 3a).

185

186 II. Quartz stage: Intense brecciation of ore stage I is followed by precipitation of the three
187 prevalent minerals of ore stage II, quartz, sphalerite, and nat. As (Fig. 3b). These minerals cement
188 the clasts of ore stage I, of pyrite (brecciated relictic pyrite inclusions in sphalerite indicate a
189 formation prior to the other stage IIa ore minerals, but after ore stage I; Fig. 4a) and of euhedral,
190 but deformed graphite (from graphite-bearing host rocks; Fig. 4b). Partial quartz pseudomorphs
191 after barite are abundant.

192 The Zn sulfides of ore stage II show two textural and mineralogical manifestations: one is
193 characterized by medium- to coarse-grained, non-colloform Zn-sulfides (mostly sphalerite; e.g.,
194 Fig. 3d) and one consists of colloform Zn-sulifdes (a mixture of both sphalerite and wurtzite,
195 confirmed by XRD; Fig. 3c). The former is more common in the southern, the latter in the

196 northern part of the vein. In the following, they are designated as colloform and non-colloform,
197 but due to their abundant similarities and irrelevance for the understanding of the behavior of
198 arsenic, most of the discussion lumps both types of Zn-sulfides together as sphalerite (sph). Both
199 types show a typical generalized sequence of quartz → jordanite/gratonite + gersdorffite +
200 sphalerite/wurtzite → sphalerite/wurtzite → galena → native arsenic → quartz (Fig. 4c-h). The
201 non-colloform variety shows a more complex mineralogy (small flakes of chalcopyrite, fahlore
202 and native bismuth are only present in the non-colloform assemblage; see Fig. 2b), but skeletal
203 jordanite/gratonite (Fig. 4c) is more abundant and formed over a longer precipitation interval in
204 the colloform compared to the non-colloform type (Fig. 4e). Furthermore, galena is more
205 common in the non-colloform ore samples (Fig. 4e, f). Small subhedral to euhedral inclusions of
206 Ni-sulfarsenide (<20μm; gersdorffite) formed during the initiation of sphalerite crystallization,
207 while round aggregates of Ni-rich triarsenide (<20 μm; skutterudite) formed subsequent to
208 sphalerite, but before the precipitation of nat. As (Fig. 3g).

209 Native As exclusively occurs in a colloform texture (irrespective of the Zn sulfide textures in the
210 same samples), overgrows all other stage II minerals (Fig. 4e, f) and in some cases embeds
211 brecciated clasts of these or fills cavities, e. g. in sphalerite-wurtzite clasts (Fig. 3h). Some native
212 arsenic aggregates (e.g., Fig. 4i) resemble the characteristic elongated shapes of Pb-sulfosalts
213 (jordanite; Fig. 4d) in sphalerite/wurzite. This texture is interpreted as native arsenic
214 pseudomorphs after Pb-sulfosalts; the same generation of nat. As overgrows sphalerite (Fig. 4i).
215 These nat. As-quartz-sphalerite associations are in some cases overgrown by another generation
216 of sphalerite that is in turn overgrown by quartz. Later breccias of all earlier mineral stages are
217 cemented by various barren quartz stages (Fig. 5a). During the final part of the quartz stage,
218 native arsenic is dissolved (Fig. 5b) and/or replaced by realgar; realgar also forms euhedral
219 crystals in cavities (Fig. 5 c, d). Rarely, the realgar crystals in cavities are in turn overgrown by

small needles of a still later second generation of nat. As (Fig. 5d). An extensive search for hydrothermal uranium-bearing minerals like uraninite or coffinite in radioactive hand specimens (as measured by a Geiger counter) produced no results, as did similar attempts by Walenta and Wimmenauer (1961). Based on the large number of fresh samples investigated by Walenta and Wimmenauer (1961) and by us (including microscopy, XRD and radiology techniques), we can exclude the presence of primary (=hydrothermal) uranium-bearing minerals in the Michael vein.

III. Carbonate stage: The occurrence of late, well-crystallized carbonates is a typical feature in many hydrothermal veins in the Schwarzwald district and records erosional uplift of the vein and near-surface conditions of formation at low temperatures (Burisch et al., 2017b). They are particularly common close to the URG (see e.g., Markl, 2017). In the Michael vein, dolomite is generally overgrown by calcite, and both fill small fractures and/or voids as euhedral crystals. No ore minerals are associated.

Supergene processes (uranium enrichment): During supergene weathering, first- and second-stage ore minerals release mainly Pb, Zn, and As and, hence, secondary minerals mainly comprise arsenates, carbonates, and sulfates of Pb and Zn, and, to a lesser extent, also of Cu (Markl, 2017). The most common supergene phases are mimetite, anglesite and cerussite, rarer, but still common phases include adamite and minerals of the beudantite-segnitite-hidalogoite series. Furthermore, an interesting suite of supergene uranium-bearing minerals exclusively occurs on fine-grained quartz III and IV (chert) samples. These include hallimondite (microcrystalline, yellow crusts), heinrichite (yellow plates), novacekite (yellow plates), hügelite (orange needles), widenmannite (yellow tabular crystals) and zeunerite (green tabular crystals)

(Fig. 5e, f; Markl, 2017). Although these minerals are relatively rare in the investigated samples, an increased radioactivity in the mine and in hand specimens from the dumps has already been detected by Kirchheimer (1957), who determined whole-rock U contents up to almost 1 wt% in some underground samples. The supergene enrichment of U is also recorded by the occasional incorporation of U in the abundant supergene mineral mimetite (Walenta and Wimmenauer, 1961). Primary U-bearing minerals are, as mentioned above, not present in the Michael vein and, hence, the uranium must have been introduced by the supergene, meteoric weathering fluids.

Analytical methods

Scanning electron microscope (SEM) & Electron-microprobe analyses (EMPA)

For qualitative mineral analyses and texture documentation, a Hitachi TM3030 REM Plus Tabletop Microscope at the University of Tübingen was used. The quantitative analysis of the minerals was carried out on 24 thin sections using a JEOL SUPERPROBE JXA - 8900RL at the University of Tübingen. To avoid tarnishing of arsenic, the thin sections were re-polished, cleaned with ethanol and dried for half a day before being spattered with carbon. Details of the analytical conditions and choice of reference materials used are described in ESM 1.

.

X-ray diffraction (XRD)

Minerals were identified based on XRD analyses using a Bruker AXS D8-Discover Co-Source diffractometer, equipped with a HOPG-monochromator and a VANTEC500 detector, at the University of Tübingen. Measurements with 50 and 300 µm diameter were performed between 5.7° to 69-100° with 0.05° and 120 sec steps at room temperature (25 °C) with a Co- Kα beam at 30 kV and 30 mA. Data evaluation was done using the DIFRACPLUSEVA software package.

Sulfur isotopes

A handpicked sample of cogenetic sphalerite and galena was powdered and the S-isotopic composition was then measured with a Finnigan Delta Plus XL mass spectrometer. The resulting S-isotopic compositions are calibrated to $\delta^{34}S$ values of several in-house standards: NBS-123 (ZnS, $\delta^{34}S$ =17.1 ‰, relative to V-CDT), NBS-127 ($BaSO_4$, $\delta^{34}S$ =20.31 ‰, relative to V-CDT), IAEA-S1 ($\delta^{34}S$ = -0.30 ‰, relative to the CDT) and IAEA-S-3 ($\delta^{34}S$ = 21.70 ‰, relative to the CDT). The long-term reproducibility of the $\delta^{34}S$ measurements is ±0.3 ‰ (2σ) and of the sulphur content it is 5 %.

Fluid inclusion analyses

For fluid inclusion analyses, several 250 μm thick, double-polished sections of quartz and sphalerite crystals were prepared. Individual fluid inclusion assemblages after Goldstein and Reynolds (1994) were characterized. No primary fluid inclusions could be detected in quartz. The only primary fluid inclusions found in any sample occur in sub- to euhedral sphalerite. They are very small (seldom larger than 10 μm) and rare. The microthermometric analyses were carried out at the University of Tübingen using a Linkam THMS 600 fluid inclusion stage on a Leica DMLP microscope calibrated with synthetic H_2O, H_2O-NaCl and H_2O-CO_2 standards. For statistical purposes, each inclusion was analyzed at least 3 times. For the homogenization temperature, a variation of less than 0.5 °C, and for melting temperatures, a variation of no more than 0.1 was accepted between runs. A pressure correction was not applied, since the salinity is unknown and a very shallow depth of formation under hydrostatic pressure can be assumed (e.g., Burisch et al., 2017b).

Thermodynamic modelling

Thermodynamic modelling was done using the software package Geochemist's Workbench 12® (GWB; Bethke, 2007). For stability diagrams, the phase 2 and P2plot GWB application and for solubility calculations during fluid cooling, the react GWB application was used. Detailed

292 information on the thermodynamic modeling approach as well as the process of thermodynamic
293 data selection for zeunerite and data estimation for jordanite and hallimondite is given in the
294 ESM 2 and the results presented in Table 2.

295

296

297 # Results
298

299 ## Mineral identification and composition

300 All ore minerals of ore stage II and some supergene minerals have been analyzed by electron
301 microprobe (crystalline sphalerite = 66 analyses, colloform sphalerite = 143, skutterudite = 7,
302 pyrite = 11, nat. As = 12, jordanite-gratonite solid-solution = 47, gersdorffite = 11, galena = 32,
303 fahlore = 30, chalcopyrite =2, realgar/pararealgar = 4, pyromorphite group minerals = 39) and
304 their respective endmember formula are given in in Table 3. The analyzed mineral compositions
305 are presented in the electronic supplementary material (ESM 3) and only some major aspects are
306 discussed here. Selected representative analysis are given in Table 4.

307 The close to ideal stoichiometric pyrite and chalcopyrite are nearly free of trace elements – only
308 Ni, Co, and As have been detected in some grains. Ni and Co are, where at all detected, very
309 close to the detection limit, but As incorporation can reach up to 0.1 wt%.

310 As explained above, Zn-sulfides have been categorized into two texturally distinct groups, the
311 colloform and non-colloform type. By X-ray diffraction, the colloform Zn-sulfide was identified
312 to be a mixture of both needle-shaped sphalerite and wurtzite. The analytical totals of all Zn-
313 sulfide measurements range from 95 to 101 with an average of 100 wt% for the non-colloform
314 and with an average of 98.5 wt% for the colloform samples. No correlation between analysis total

and stoichiometry of the calculated formula exists, the variations in totals reflect variations in porosity. However, for interpretation, only analyses with a total between 98 and 101 wt% have been considered. Elevated Pb and As concentrations in both types of sphalerites (Table 4) indicate the presence of jordanite-gratonite solid-solution microinclusions in sphalerite; they are more common in the colloform textures (Fig. 6). This compositional argument is supported by the close association of visible jordanite-gratonite solid-solution bands within the colloform sphalerite. Sub-microscopic inclusions of other sulfides in sphalerite have been previously reported from other localities (e.g., Taylor and Radtke, 1969; Kelley et al., 2004; Pfaff et al., 2011). Besides Pb and As, the sphalerite of both textural types is generally poor in trace elements and only Cd can be present up to 3.5 wt% in a handful of analyses. Sphalerite contains generally << 1 wt% Fe and shows the transparent reddish to brownish color typical of Fe-poor varieties. The analyzed galena has a stoichiometric formula and lacks trace elements.

X-ray diffraction and compositional analyses revealed the presence of both jordanite (ideally $Pb_{14}(As,Sb)_6S_{23}$) and gratonite (ideally $Pb_9As_4S_{15}$). Both minerals are commonly intergrown and embedded within the colloform sphalerite. The only significant trace element is Zn, which can reach values of up to several wt% (but this may be due to microinclusions again, see above). Due to their small grain size, no gersdorffite and almost no skutterudite grains could be analyzed without contamination by galena and/or sphalerite. However, such mixed analyses still indicate their ternary nature with respect to Fe, Co, and Ni (0.2 : 0.15 : 1 and 0.54 : 0.3 : 1 for skutterudite and gersdorffite, respectively). Furthermore, gersdorffite is enriched in Se (ca. 0.2 wt%). The fahlore is a near endmember Cu-Zn-tennantite with an average mineral formula of $Cu_{10.02}Fe_{0.33}Zn_{1.52}As_{3.88}Sb_{0.09}S_{13.15}$. Native As incorporates up to 0.2 wt% Zn, 0.4 wt% Pb, and 0.6 wt% Se and Sb each. In all these As-bearing minerals, other trace elements are close to or below the detection limit.

Realgar/pararealgar shows a similar trace element budget as nat. As, and is enriched in Sb and Se. The pyromorphite group minerals of the Michael vein are commonly close to endmember mimetites. Occasionally, however, phosphate substitution in individual crystals is high enough to reach pyromorphite composition. The Ca content rarely reaches 0.2 wt%. Uranium is generally absent, but individual analyses can reach up to 1 wt% UO_2 (Table).

Temperature of formation

To constrain the temperature of formation of the stage II mineralization, two independent thermometers were applied: sulfide isotope equilibrium and fluid inclusion homogenization. For the isotope analyses, the cogenetic minerals (colloform sphalerite/wurtzite mixture and galena (KS13)) were carefully isolated and hand-picked. The sphalerite has a $\delta^{34}S$-value (V-CDT, ‰) of -3.68(0.3) and the galena of -8.58(0.3). Applying the isotope fractionation factors of Seal (2006 and references therein), and assuming the literature isotope fractionation factor for ZnS applies to both wurtzite and sphalerite, the resulting calculated equilibrium temperature is approx. 110(20) °C (Gauss uncertainty propagation). The eight primary fluid inclusions analyzed in non-colloform sphalerite (100, 102, 104, 109, 110, 119, 123, 128 °C) nicely support this result: they indicate a homogenization temperature range of 100-128 °C with an average of approx. 110(10) °C (1σ).

Due to the formation of metastable phases at low temperatures in the fluid inclusions, the salinity of the primary fluid inclusions in sphalerite could not be quantitatively determined – but it could still be qualitatively constrained to some degree. The approximate temperature of first melting is around -50 °C. In combination with the presence of abundant hydrohalite, this constrains the fluid

to be of high salinity with an at least ternary composition ($NaCl$-$CaCl_2$-H_2O). The presence of hydrohalite and the absence of Ca-chlorides documents a possible NaCl dominance over $CaCl_2$.

Thermodynamic modelling and fluid constraints

The highly saline and most probably NaCl-dominated fluid is in good agreement with typical fluid inclusion analyses from veins related to Upper-Rhine-Graben tectonics (5-25 wt% $NaCl+CaCl_2$ Walter et al., 2018). For thermodynamic modeling, we used an intermediate salinity of 10 wt% NaCl. Based on the above temperature estimations, and because sphalerite precipitation is commonly preceded by some quartz crystallization in ore stage II, it is estimated that mineral precipitation occurred between 150 and 50 °C, with most of the ore minerals probably precipitating between 130 °C and 90 °C.

The elemental fluid composition for the thermodynamic modelling is based on qualitative constraints, empirical calculations and a literature compilation/comparison. The precipitation mechanism for quartz is assumed to be fluid cooling and for the sulfides to be reduction related to the influx of a sulfide-rich fluid. At close to neutral *pH* (neutral ±2), 1 kg of H_2O fluid cooled from 150 to 50 °C can precipitate ca. 150 mg SiO_2. Based on the estimated abundance of the major minerals in ore stage II (quartz 90 vol%, sphalerite 7 vol% and nat. As 3 vol%), the amount of sphalerite and nat. As that has to precipitate from 1 kg of fluid can be calculated (ca. 20 mg and 10 mg/kg respectively). This implies that the fluid must have contained at least 10 mg/kg Zn and As, respectively. Furthermore, for the whole mineral sequence to form, Zn has to be successively depleted relative to sulfide. Thus, the calculated 10 mg/kg of Zn is not a minimum but a rough absolute estimate. Assuming the relative abundance of Zn, Pb and Ni in the

mineralization, we estimate the fluid composition to be roughly 10 mg/kg of Zn and As, 1 mg/kg of Pb, and 0.1 mg/kg of Ni. This composition is in very good agreement with naturally occurring Upper-Rhine-Graben brines which are related to the Buntsandstein aquifer: such brines contain up to 10 mg/kg Zn and As each, up to 1 mg/kg Pb and up to 0.1 mg/kg Ni (Sanjuan et al., 2010).

Discussion

Precipitation mechanism

The first mineralization stage with barite and galena is a very common type of mineralization in the vicinity of the URG (e.g., Metz and Richter, 1957; Markl, 2015; Markl, 2017) and formed by a three component fluid mixing process involving a metal-bearing basement-derived, a sulfate-bearing sedimentary cover-derived and a sulfide-bearing fluid (e.g., Walter et al., 2018).

In contrast, the subsequent nat. As-sphalerite-quartz stage II is a regionally unique and worldwide rare type of mineralization. Hence, it needed very special conditions of formation, which are, obviously, only rarely fulfilled in nature. The large quantities of fine-grained crystalline quartz indicate that cooling was the dominant precipitation mechanism. This is supported by textures, i.e. the typical pseudomorphs of quartz after barite (Burisch et al., 2017c) and nat. As after jordanite/gratonite. Fluid cooling does not, however, explain the amount of sphalerite present relative to quartz, as the decrease of sphalerite solubility with temperature is minimal in the investigated temperature range of 150-50 °C (e.g., Hayashi et al., 1990; Hanor, 1996). Native arsenic precipitation has been proposed to be facilitated by a decrease in temperature, pressure, and most importantly fO_2 (e.g., Su et al., 2009; Zheng et al., 2015; Markl et al., 2016; Burisch et al., 2017a; Scharrer et al., 2019). Thus, even though fluid cooling promotes some precipitation of sphalerite and nat. As, an influx of a redox agent is needed to precipitate the whole sequence of

minerals in the observed quantities. The presence of abundant nat. As (As^{0}) and some arsenides (As^{-II}) in combination with the absence of graphite dissolution textures in the samples (Fig. 4b) demonstrates a strongly reduced environment during the formation of the ores. Due to the presence of abundant sulfides and the slow kinetics of sulfate to sulfide reduction in the observed temperature range (Sakai, 1968; Malinin and Khitarov, 1969; Rye and Ohmoto, 1974; Ohmoto and Lasaga, 1982), it is most likely that an influx of sulfide was essential. An abiotic in situ reduction of sulfate to sulfide can be excluded since the most abundant source of sulfate present is the partially dissolved barite, which at approx. 100 °C is in strong isotopic disequilibrium with the sphalerite (Schwinn et al., 2006; Seal, 2006). It has been proposed that colloform sphalerite can form by mixing of a fluid containing bacteriogenic sulfur and a metal-bearing hydrothermal fluid (Wilkinson et al., 2005; Barrie et al., 2009; Pfaff et al., 2011). Bacteriogenic sulfate reduction has been proven to prevail to temperatures up to 110 °C with an optimal range of 30-40 °C (e.g., Jørgensen et al., 1992; Seal, 2006). Thus, groundwater sulfate reduction is a possible sulfide source for the mineralization in question. Other possible sources of sulfide are magmatic or metamorphic sulfides from the host rocks, diagenetic/sedimentary sulfides, or URG oil field brines. In summary, a combination of fluid cooling and the influx of a sulfide and/or possibly other redox agents was responsible for the formation of the sphalerite-nat. As-quartz stage II assemblage. This, however, does not explain the uniqueness of the abundance of native arsenic in this mineralization, as the combination of reducing conditions in the presence of aqueous arsenic is probably not very rare; most As-rich associations are sulfide, sulfarsenide or arsenide dominated and completely lack or are very poor in nat. As (e.g., most five element deposits, Scharrer et al., 2019 and references therein).

Conditions of formation

Thermodynamic calculations show that at roughly neutral pH, the paragenetic sequence of ZnS + galena + Pb-As-sulfosalts → nat. As, the precipitation of the Ni sulfarsenide (gersdorffite) during sphalerite formation and the arsenide formation at the transition to the nat. As formation can be nicely reproduced using the element concentrations discussed above (Fig. 7). However, this only explains that it is thermodynamically possible to form this mineralization by a fluid mixing/reduction/sulfide influx scenario. It does, however, not explain the scarcity of native arsenic in base-metal mineralizations in general. Normally, arsenic is almost exclusively stored in other, significantly more common minerals such as arsenopyrite, As-rich pyrite, sulfosalts, and arsenides.

The important parameters constraining a nat. As-bearing base-metal mineralization to form are summarized here (Fig. 8) and further discussed in the following sub-chapters. Obviously, it is essential for the mineralizing fluid to contain sufficient Zn, Pb, S, and As. However, for native arsenic to form, it is crucial that the transition elements Ni, Co, and Fe have very low concentrations, as otherwise sulfarsenides and/or arsenides would form instead of nat. As (see below). A lower temperature favors nat. As stability, but it also favors the formation of realgar and orpiment. The stability of these As-sulfides is, however, suppressed at roughly neutral conditions by the abundance of dissolved metals such as Zn and Pb which limit the availability of sulfide.

Low concentrations of Fe, Co, and Ni. In hydrothermal systems, such as base metal mineralizations, arsenic most commonly precipitates as arsenopyrite or gersdorffite, while native arsenic is comparatively rare (approx. 10.000 vs. 400 occurrences worldwide, Mindat.org). To

promote the formation of nat. As instead of arsenopyrite, either sulfide or iron has to be limited. Since nat. As also occurs in sulfide/sulfosalt-rich mineralizations (e.g., Bailly et al., 1998; An and Zhu, 2009; Su et al., 2009; Radosavljević et al., 2014), and as this is also in the present situation the case, sulfide is most likely not the defining factor. The assumption of low concentrations of Fe, Co, and Ni in the mineralizing fluid during nat. As crystallization is in accordance with many textural observations, as native arsenic typically precipitates after the precipitation of theses transition metals (Noble, 1950; McKinstry, 1963; Bailly et al., 1998; Su et al., 2009; Zheng et al., 2015; Scharrer et al., 2019). Thus, it is likely that these metals were depleted by the time the reducing conditions allowed nat. As to precipitate.

Thermodynamic calculations show, in general, that for nat. As to form the fluid has to be either extremely acidic or deprived of Fe, Co, and Ni relative to As, since, otherwise, the sulfarsenides or arsenides would form (Fig. 9). Strongly acidic conditions can be excluded based on the presence of sphalerite and galena (stable at pH > approx. 3; 100 °C) and the lack of dissolution textures of these phases during nat. As precipitation. The absence of the transition elements Fe, Co, and Ni in the Michael vein is also recorded by the observed mineralogy (Fig. 2). Co-and Ni-bearing minerals are very rare, their crystals are tiny and the only relevant Fe-bearing minerals in the mineralization are scarce pyrite grains and the abundant, but conspicuously Fe-poor sphalerite (commonly significantly less than 1 mol% Fe). The Fe-Zn substitution in sphalerite means that from a fluid precipitating 10 mg/kg of Zn in the form of sphalerite, less than 0.1 mg/kg of Fe is co-precipitated. Hence, the fluid was iron-poor already prior to sphalerite formation.

In contrast to Ni and Co, Fe is omnipresent in all lithological units in the region and, hence, every hydrothermal fluid should contain abundant Fe (dependent on redox and pH state, however). This is recorded by the common presence of pyrite, arsenopyrite and/or chalcopyrite in most

hydrothermal veins of the region (e.g., Metz and Richter, 1957; Bliedtner and Martin, 1986), by the presence of iron in thermal spring fluids (0.01-10 mg/kg; Göb et al., 2013) and by hydrothermal fluid inclusions of the region (up to approx. 10 000 mg/kg; Walter et al., 2018). Thus, for the case at hand, either the transport of Fe is retarded by, for example, the stability of hematite and/or Fe-oxyhydroxides at neutral to basic *pH* or the initially present Fe had been precipitated prior to the formation of the Fe-poor mineralization of stage IIa. The latter would explain the presence of brecciated clasts of pyrite occasionally embedded in sphalerite, which could be more abundant at depth. Furthermore, the lack of trace elements (nearly all below the detection limit) indicates a low temperature formation of pyrite and not a remobilization of host rock pyrite and the lack of these clasts within stage I minerals indicates a formation after stage I but before stage IIa. However, at present we cannot distinguish whether the fluid was primarily Fe-poor or if significant pyrite precipitation occurred at greater depth which depleted the fluid in iron. It is, however, clear that if sulfarsenides are absent, very low Fe concentrations are essential for this nat. As-rich base metal mineralization to form.

Temperature, sulfur abundance and the stability of nat. As. The solubility of all minerals in question decreases with decreasing temperature (Fig. 10) and, hence, the formation of mineral assemblage IIa is favored by and related to fluid cooling. Furthermore, nat. As is only stable at < approx. 300 °C (at low pressure) and becomes increasingly stable at lower temperatures. The even more significant temperature dependence of the realgar and orpiment stability field relative to nat. As (Fig. 10) explains the late-stage overprint of nat. As by realgar which is also typical of nat. As occurrences worldwide (e.g., Bailly et al., 1998; Cleverley et al., 2003). The increased stability of As-minerals at lower temperature explains the generally described correlation

between arsenic content and temperature in hydrothermal fluids and springs (e.g., Ballantyne and Moore, 1988; Aiuppa et al., 2003).

Although lower temperatures favor the formation of nat. As, they also favor the formation of realgar and orpiment in the presence of sulfide. This explains the more common presence of realgar over nat. As in cooler and/or high sulfidation mineralizations (e.g., Arehart et al., 1993; Migdisov and Bychkov, 1998; Cleverley et al., 2003; Su et al., 2009; Zhu et al., 2011). It is essential to understand the stability of realgar and orpiment, since these are absent during the precipitation of the main ore phases of stage II, and their lack of stability promotes the formation of nat. As. The stability of realgar/orpiment is confined to low temperatures, an acidic to neutral pH, and by the availability of both As and sulfide (e.g., Sergeyeva and Khodakovskiy, 1969; Ballantyne and Moore, 1988, Fig. 10, Fig. 11). The availability of sulfide is, however, not only defined by the absolute abundance of S or kinetic disequilibrium between sulfate and sulfide (Scharrer et al., 2019) in the fluid, but also by the abundance of metals. The presence of transition metals such as Pb and Zn limits the availability of sulfur at reducing conditions by the precipitation of sulfides (Fig. 11). This interdependence, variable affinity of different elements to sulfur (Shcherbina, 1978), enables the precipitation of nat. As in the presence of sulfide; e.g. in roughly neutral fluids at 100 °C containing approx. 10 mg/kg or 100 mg/kg of Zn or Pb at least 5-15 mg/kg (depending on As content) or 50 mg/kg of sulfur is needed, respectively, for realgar/orpiment to form instead of nat. As (e.g., Fig. 11). A fluid containing >1000 mg/kg of these base metals would need an unrealistically high amount of sulfur (>>1000 mg/kg) to form realgar, even at high arsenic contents (>1000 mg/kg). Thus, the availability of abundant Zn or Pb in a sulfide-rich environment, as is the case for the Michael vein, decreases the stability of the As-sulfides and thus promotes nat. As formation.

523

524 **Native arsenic as a trap for uranium during supergene processes**

525 Generally, low temperature uranium deposits/ enrichments form by either by reduction of
526 dissolved U^{+VI} to U^{+IV} or by sorption at strongly acidic pH, where U^{+VI} may also be subsequently
527 reduced (Langmuir, 1978; Dahlkamp, 2009; Dahlkamp, 2013). Typical reducing agents are for
528 example organic material, sulfide, or pyrite (Andreev and Chumachenko, 1964; Sharp et al.,
529 2011; Dahlkamp, 2013). During supergene overprinting of such primary uranium bearing
530 associations, U^{+IV} is re-oxidized, during which, uranyl-bearing minerals form (e.g., Finch and
531 Ewing, 1991; Gorman-Lewis et al., 2008). This is however not the case for the Michael vein. The
532 Michael vein is quite unique as it contains a wealth of supergene uranium-bearing minerals
533 (including rare Pb- bearing uranylarsenates, while primary uranium minerals such as uraninite are
534 missing entirely (this study, Walenta and Wimmenauer, 1961). Thus, uranium is present
535 exclusively as U^{+VI} both in Ba-, Pb-, Cu-, and Mg-uranyl arsenates and as a minor constituent in
536 mimetite. In some places along the vein, the accumulations of supergene uranium-bearing
537 minerals result in significant whole-rock uranium contents up to 1 wt% (Kirchheimer, 1957).

538 Due to the lack of primary, U^{+IV}-bearing uranium bearing minerals, the supergene uranyl
539 minerals must have directly precipitated from a U^{+VI}-bearing fluid where the mineralized vein
540 acted as the uranium trap (Fig. 12a). The most likely source of uranium is the granitic host rock,
541 which is slightly enriched in uranium (Martin, 2009; Dahlkamp, 2013). The release of uranium
542 from such rocks to the fluid by weathering is indicated by the presence of uranium in granitic
543 formation waters from southwest Germany (occasionally up to 30 µg/kg; Käß and Käß, 2008;
544 Göb et al., 2013) and the lower uranium concentration in altered granite compared to fresh
545 granite in the Schwarzwald (e.g., Hofmann, 1989). Although nat. As has a strong reduction
546 potential, it did not directly act as a uranium immobilization agent by U^{+VI} reduction. However,

547 during weathering and oxidation of the vein system, the arsenic in the nat. As is oxidized, which
548 can then react with the uranyl bearing fluid to form the uranylarsenates. The, for the
549 uranylarsenates also needed, metal ions (e.g., Cu, Pb, Ba) are provided by weathering and
550 dissolution of gangue minerals such as galena, chalcopyrite and barite. It has been argued that
551 U^{+VI} sorption can limit the solubility of uranium even though the stabilities of uranyl arsenates
552 are not reached (Langmuir, 1978) and that sorption may be a precursor step to the local
553 enrichment of uranium/formation of uranyl minerals (Barton, 1956). This, however, seems not to
554 be the case in the Michael vein, since the uranyl-bearing minerals form exclusively in quartz vugs
555 and on fractures independent of typical adsorbents such as ferric oxides, hydroxides or organic
556 material. Thus, we assume a direct precipitation from the fluid due to oversaturation of the
557 respective uranyl arsenates by small-scale fluid mixing of compositionally contrasting fluids that
558 reacted with variable amounts of the host rock and gangue minerals, etc. (Fig. 12a).

559 The dominance of uranyl arsenates over phosphates or silicates can be explained by the relatively
560 high solubility of the latter two (Langmuir, 1978). Still, the formation of such an abundance of
561 uranyl arsenates is an abnormal scenario, as dissolved phosphate and silicate is naturally much
562 more common than arsenate under supergene conditions in "common" surface waters (e.g.,
563 Johnson, 1971; Göb et al., 2013). In the present case, though, arsenates are stabilized by the high
564 arsenate concentrations released during supergene weathering of native arsenic, from which
565 several orders of magnitude more is needed than phosphor to produce arsenates instead of
566 phosphate (Fig. 12). The formation of the uranyl minerals is further promoted by other
567 parameters, such as pH and temperature. The typical weathering fluids and mine drainage fluids
568 in the Schwarzwald have an ideal pH (average of pH 6; Göb et al., 2013) for uranyl mineral
569 formation as it coincides with the pH of lowest uranyl solubility and the stability of most

570 important uranyl minerals (pH range from 5 to 8.5 Langmuir, 1978). This pH rang is also
571 roughly the stability boundary for both zeunerite and hallimondite at the given conditions.

572 Although uranyl arsenates are generally less common than, for example, uranyl phosphates or
573 silicates, their general occurrence is nothing unusual. Extremely rare, however, is the formation
574 of Pb-bearing uranyl arsenates such as hallimondite and hügelite. Both have less than 10
575 occurrences worldwide (mindat.org) and their type locality is the Michael vein. Their stability is
576 normally limited by the highly insoluble Pb-arsenate mimetite which is an extremely common
577 mineral with thousands of occurrences worldwide. The stability of mimetite, however, is strongly
578 dependent on the Cl-content of the fluid (Fig. 12c). Accordingly, the Pb-uranyl arsenates form
579 due to the presence of sufficient Pb and As (supplied by the weathered hypogene minerals galena
580 and nat. As) combined with the depletion of Cl. The initial Cl-content of mine waters is
581 commonly in the range of 0.5-50 mg/kg (Göb et al., 2013). Due to the abundance of nat. As and
582 galena in the vein, mimetite is the most abundant supergene mineral of the Michael vein. The
583 precipitation of mimetite successively depletes the fluid in Cl, which enables the formation of Pb-
584 uranyl arsenates (Fig. 12c). Finally, the quite common occurrence of the Cu uranyl arsenate
585 zeunerite in the almost Cu-free Michael vein needs some explanation. Primary Cu-bearing
586 minerals such as chalcopyrite are not absent, but very rare in the Michael vein, and hence,
587 zeunerite was not expected to form in such an environment. However, due to the significantly
588 lower solubility of zeunerite relative to Pb-uranyl arsenates (clearly visible, even when
589 considering the large solubility uncertainty of hallimondite), zeunerite forms at a very low Cu
590 content, if the arsenate content of a fluid is high (Fig. 12d).

591

This is a preprint, the final version is subject to change, of the American Mineralogist (MSA)
Cite as Authors (Year) Title. American Mineralogist, in press.
DOI: https://doi.org/10.2138/am-2020-7062

Implications

The nat. As-bearing mineralization stage of the Michael vein is a prime example to study the mobility and precipitation mechanism of arsenic not only in hydrothermal base metal veins, but many other types of hydrothermal environments. The requirements for nat. As formation can be summarized as follows:

1. the availability of abundant aqueous arsenic,
2. reduced conditions,
3. very low concentrations of the transition metals Fe, Co and Ni,
4. very low sulfide concentrations (which can be reached by a lack of sulfide or presence of significant amounts of transition elements such as Pb and Zn).

If these requirements are met (which rarely occurs in nature), nat. As can form in large masses and can become a substantial part of a mineralization. These conditions not only provide insight on the formation of nat. As, but also on the absence of nat. As and presence of other As-bearing minerals which is important to understand the fate of (toxic) arsenic in natural environments. If for example condition 3 is not fulfilled, the resulting mineralization is arsenide-dominated, which is typical of the native element-arsenide (five element) type of deposit (Bastin, 1939; Kissin, 1992; Markl et al., 2016; Scharrer et al., 2019). If condition 4 is not achieved, the result is a realgar-orpiment mineralization, such as the geothermal fields of Uzon, Russia (Migdisov and Bychkov, 1998; Cleverley et al., 2003) or the As-mineralization at Saualp, Austria (Göd and Zemann, 2000). If both Fe and sulfide are abundantly present, the resulting dominant As-mineral is arsenopyrite, which is common in most other As-bearing hydrothermal mineralizations.

The initial lack of nat. As stability during ore formation by a predominating stability of other As-bearing minerals does not exclude the late stage formation of nat. As. A relative abundance of dissolved arsenic over dissolved Fe, Co, Ni and S and their depletion during ore precipitation can lead to a saturation of nat. As. This explains the general late-stage occurrence of nat. As (e.g., Su et al., 2009; Zheng et al., 2015; Scharrer et al., 2019). This late-stage nat. As formation is further facilitated by lower temperatures.

If condition two (reduced environment) is not given, the mineralization is dominated by highly insoluble arsenate minerals. Such an environment is, for example, produced by weathering of nat. As-bearing mineralizations. The presence of nat. As and its highly reactive nature under oxidized conditions can act as a natural barrier for uranium (U^{+VI}) dissolved in ground water where native arsenic becomes oxidized to arsenate and forms a variety of different uranyl arsenates, depending on the availability of metals such as Pb, Cu, or Ba. The insoluble nature of these uranyl arsenates enables them to form at even low uranium concentrations (approx. 1 µg/kg) as are typical of the granitic aquifers of the region (Käß and Käß, 2008; Göb et al., 2013). This shows that nat. As-rich mineralizations can act as a natural trap for U from groundwater.

Acknowledgements

We thankfully acknowledge Manfred Martin and the Landesamt für Geologie, Rohstoffe und Bergbau (LRGB) for providing unique and historic samples from the Geological Survey of Baden-Württemberg. Furthermore, we thank Tatjana Epp and Thomas Wenzel for beneficial feedback on textural and genetic interpretations. An anonymous reviewer and associate editor Thomas Mueller are thanked for constructive feedback. Moreover, we thank Simone Schafflick

637 and Per Jeiseke for sample preparation. A significant part of this research was achieved due to the
638 DFG grant MA 2135/25-1.

639

640 ## References
641

642 Aiuppa, A., D'Alessandro, W., Federico, C., Palumbo, B., and Valenza, M. (2003) The aquatic geochemistry
643 of arsenic in volcanic groundwaters from southern Italy. Applied Geochemistry, 18(9), 1283-
644 1296.
645 Amend, J.P., Saltikov, C., Lu, G.-S., and Hernandez, J. (2014) Microbial arsenic metabolism and reaction
646 energetics. Reviews in Mineralogy and Geochemistry, 79(1), 391-433.
647 An, F., and Zhu, Y. (2009) Significance of native arsenic in the Baogutu gold deposit, western Junggar,
648 Xinjiang, NW China. Chinese Science Bulletin, 54(10), 1744.
649 Andreev, P., and Chumachenko, A. (1964) Reduction of uranium by natural organic substances.
650 Geochem. Int., 1: 3-7 (1964).(1), 3-7.
651 Arehart, G.B., Chryssoulis, S.L., and Kesler, S.E. (1993) Gold and arsenic in iron sulfides from sediment-
652 hosted disseminated gold deposits; implications for depositional processes. Economic Geology,
653 88(1), 171-185.
654 Bailly, L., Milesi, J.-P., Leroyb, J., and Marcouxa, E. (1998) The Au-Cu-Zn-Sb epithermal mineralisations of
655 the Baia Mare district (North Romania): new mineralogical and microthermometric results.
656 Comptes Rendus de l'Académie des Sciences-Series IIA-Earth and Planetary Science, 327(6), 385-
657 390.
658 Ballantyne, J.M., and Moore, J.N. (1988) Arsenic geochemistry in geothermal systems. Geochimica et
659 Cosmochimica Acta, 52(2), 475-483.
660 Barrie, C.D., Boyce, A.J., Boyle, A.P., Williams, P.J., Blake, K., Wilkinson, J.J., Lowther, M., McDermott, P.,
661 and Prior, D.J. (2009) On the growth of colloform textures: a case study of sphalerite from the
662 Galmoy ore body, Ireland. Journal of the Geological Society, 166(3), 563-582.
663 Barton, P.B. (1956) Fixation of uranium in the oxidized base metal ores of the Goodsprings district, Clark
664 County, Nevada. Economic Geology, 51(2), 178-191.
665 Bastin, E.S. (1939) The nickel-cobalt-native silver ore type. Economic Geology, 34(1), 40-79.
666 Bethke, C.M. (2007) Geochemical and biogeochemical reaction modeling. 564 p. Cambridge University
667 Press.
668 Bliedtner, M., and Martin, M. (1986) Erz-und Minerallagerstätten des mittleren Schwarzwaldes. Geol.
669 Landesamt Baden-Württemberg.
670 Boitsov, V., and Kaikova, T. (1965) Uranium and arsenic in the hydrothermal process. Soviet Atomic
671 Energy, 18(4), 473-479.
672 Bowell, R.J., Alpers, C.N., Jamieson, H.E., Nordstrom, D.K., and Majzlan, J. (2014) The environmental
673 geochemistry of arsenic: an overview. Reviews in Mineralogy and Geochemistry, 79(1), 1-16.
674 Bowell, R.J., and Craw, D. (2014) The management of arsenic in the mining industry. Reviews in
675 Mineralogy and Geochemistry, 79(1), 507-532.
676 Burisch, M., Gerdes, A., Walter, B.F., Neumann, U., Fettel, M., and Markl, G. (2017a) Methane and the
677 origin of five-element veins: Mineralogy, age, fluid inclusion chemistry and ore forming
678 processes in the Odenwald, SW Germany. Ore Geology Reviews, 81, 42-60.

679 Burisch, M., Walter, B.F., Gerdes, A., Lanz, M., and Markl, G. (2017b) Late-stage anhydrite-gypsum-
680 siderite-dolomite-calcite assemblages record the transition from a deep to a shallow
681 hydrothermal system in the Schwarzwald mining district, SW Germany. Geochimica et
682 Cosmochimica Acta, 223, 259-278.
683 Burisch, M., Walter, B.F., and Markl, G. (2017c) Silicification of Hydrothermal Gangue Minerals in Pb-Zn-
684 Cu-fluorite-quartz-baryte Veins. The Canadian Mineralogist, 55(3), 501-514.
685 Burisch, M., Walter, B.F., Wälle, M., and Markl, G. (2016) Tracing fluid migration pathways in the root
686 zone below unconformity-related hydrothermal veins: Insights from trace element systematics
687 of individual fluid inclusions. Chemical Geology, 429, 44-60.
688 Cerny, P., and Harris, D. (1978) The Tanco pegmatite at Bernic Lake, Manitoba; XI, Native elements,
689 alloys, sulfides and sulfosalts. The Canadian Mineralogist, 16(4), 625-640.
690 Cleverley, J.S., Benning, L.G., and Mountain, B.W. (2003) Reaction path modelling in the As–S system: a
691 case study for geothermal As transport. Applied Geochemistry, 18(9), 1325-1345.
692 Cook, N.J. (1996) Mineralogy of the sulphide deposits at Sulitjelma, northern Norway. Ore Geology
693 Reviews, 11(5), 303-338.
694 Criaud, A., and Fouillac, C. (1989) The distribution of arsenic (III) and arsenic (V) in geothermal waters:
695 Examples from the Massif Central of France, the Island of Dominica in the Leeward Islands of the
696 Caribbean, the Valles Caldera of New Mexico, USA, and southwest Bulgaria. Chemical geology,
697 76(3-4), 259-269.
698 Dahlkamp, F.J. (2009) Uranium deposits of the world. Springer Science & Business Media.
699 -. (2013) Uranium ore deposits. 460 p. Springer Science & Business Media.
700 Drahota, P., and Filippi, M. (2009) Secondary arsenic minerals in the environment: a review. Environment
701 International, 35(8), 1243-1255.
702 Dudas, M. (1987) Accumulation of native arsenic in acid sulphate soils in Alberta. Canadian Journal of Soil
703 Science, 67(2), 317-331.
704 Epp, T., Walter, B., Scharrer, M., Lehmann, G., Henze, K., Heimgärtner, C., Bach, W., and Markl, G. (2018)
705 Quartz veins with associated Sb-Pb-Ag±Au mineralization in the Schwarzwald, SW Germany: a
706 record of metamorphic cooling, tectonic rifting, and element remobilization processes in the
707 Variscan belt. Mineralium Deposita, 1-26.
708 Essarraj, S., Boiron, M.-C., Cathelineau, M., Banks, D.A., and Benharref, M. (2005) Penetration of surface-
709 evaporated brines into the Proterozoic basement and deposition of Co and Ag at Bou Azzer
710 (Morocco): Evidence from fluid inclusions. Journal of African Earth Sciences, 41(1), 25-39.
711 Finch, R., and Ewing, R. (1991) Alteration of natural UO2 under oxidizing conditions from Shinkolobwe,
712 Katanga, Zaire: A natural analogue for the corrosion of spent fuel. Radiochimica Acta, 52(2), 395-
713 402.
714 Fusswinkel, T., Wagner, T., Wenzel, T., Wälle, M., and Lorenz, J. (2014) Red bed and basement sourced
715 fluids recorded in hydrothermal Mn–Fe–As veins, Sailauf (Germany): A LA-ICPMS fluid inclusion
716 study. Chemical Geology, 363, 22-39.
717 Geyer, O.F., Gwinner, M.P., Geyer, M., Nitsch, E., and Simon, T. (2011) Geologie von Baden-
718 Württemberg. Schweizerbart.
719 Glaskova, O., Azaroual, M., and Piantone, P. (1999) Arsenic behaviour in subsurface hydrogeochemical
720 systems(a critical review of thermodynamic data for minerals and aqueous species of arsenic).
721 Göb, S., Loges, A., Nolde, N., Bau, M., Jacob, D.E., and Markl, G. (2013) Major and trace element
722 compositions (including REE) of mineral, thermal, mine and surface waters in SW Germany and
723 implications for water–rock interaction. Applied Geochemistry, 33, 127-152.
724 Göd, R., and Zemann, J. (2000) Native arsenic–realgar mineralization in marbles from Saualpe, Carinthia,
725 Austria. Mineralogy and Petrology, 70(1-2), 37-53.
726 Goldstein, H., and Reynolds, T. (1994) Systematics of fluid inclusions in diagenetic minerals. SEPM short
727 course, 31, 199.

Gorman-Lewis, D., Burns, P.C., and Fein, J.B. (2008) Review of uranyl mineral solubility measurements. The Journal of Chemical Thermodynamics, 40(3), 335-352.

Grancea, L., Bailly, L., Leroy, J., Banks, D., Marcoux, E., Milési, J., Cuney, M., André, A., Istvan, D., and Fabre, C. (2002) Fluid evolution in the Baia Mare epithermal gold/polymetallic district, Inner Carpathians, Romania. Mineralium Deposita, 37(6-7), 630-647.

Hanor, J.S. (1996) Controls on the solubilization of lead and zinc in basinal brines. Carbonate-hosted Lead–Zinc Deposits, SEG Special Publication: USA, 4, 483-500.

Hayashi, K., Sugaki, A., and Kitakaze, A. (1990) Solubility of sphalerite in aqueous sulfide solutions at temperatures between 25 and 240 °C. Geochimica et Cosmochimica Acta, 54(3), 715-725.

Hiller, A., and Schuppan, W. (2008) Geologie und Uranbergbau im Revier Schlema-Alberoda. Bergbau in Sachsen, 14, p. 200. Landesamt für Umwelt, Landwirtschaft und Geologie.

Hofmann, B. (1989) Genese, Alteration und rezentes Fliess-System der Uranlagerstätte Krunkelbach (Menzenschwand, Südschwarzwald), PhD, p. 195. Universität Bern.

Hofmann, B., and Knill, M. (1996) Geochemistry and genesis of the Lengenbach Pb-Zn-As-Tl-Ba-mineralisation, Binn Valley, Switzerland. Mineralium Deposita, 31(4), 319-339.

Horton, T.W., Becker, J., Craw, D., Koons, P., and Chamberlain, C.P. (2001) Hydrothermal arsenic enrichment in an active mountain belt: Southern Alps, New Zealand. Chemical Geology, 177(3-4), 323-339.

Hösel, G. (2003) Die polymetallische Skarnlagerstätte Pöhla-Globenstein. Bergbau in Sachsen, 8, p. 147. Landesamt für Umwelt, Landwirtschaft und Geologie.

Johnson, D.L. (1971) Simultaneous determination of arsenate and phosphate in natural waters. Environmental Science & Technology, 5(5), 411-414.

Jørgensen, B.B., Isaksen, M.F., and Jannasch, H.W. (1992) Bacterial sulfate reduction above 100 C in deep-sea hydrothermal vent sediments. Science, 258(5089), 1756-1757.

Kaiser, H. (1983) Die Mineralien der Grube Michael, Weiler bei Lahr, Schwarzwald. Lapis, 8(12).

Käß, W., and Käß, H. (2008) Deutsches Bäderbuch [Manual of spa therapy and german spas]. Schweizerbart.

Keller, N.S., Stefánsson, A., and Sigfússon, B. (2014) Arsenic speciation in natural sulfidic geothermal waters. Geochimica et Cosmochimica Acta, 142, 15-26.

Kelley, K., Leach, D., Johnson, C., Clark, J., Fayek, M., Slack, J., Anderson, V., Ayuso, R., and Ridley, W. (2004) Textural, compositional, and sulfur isotope variations of sulfide minerals in the Red Dog Zn-Pb-Ag deposits, Brooks Range, Alaska: Implications for ore formation. Economic Geology, 99(7), 1509-1532.

Kesler, S.E., Fortuna, J., Ye, Z., Alt, J.C., Core, D.P., Zohar, P., Borhauer, J., and Chryssoulis, S.L. (2003) Evaluation of the role of sulfidation in deposition of gold, Screamer section of the Betze-Post Carlin-type deposit, Nevada. Economic Geology, 98(6), 1137-1157.

Kirchheimer, F. (1957) Bericht über das Vorkommen von Uran in Baden-Württemberg. Kommissionsverlag von Herder.

Kissin, S.A. (1992) Five-element (Ni-Co-As-Ag-Bi) veins. Geoscience Canada, 19(3), 113-124.

Krahé, L. (2012) Geochemische und mineralogische Untersuchungen am Erzgang Michaelgang bei Lahr. Geoscience, Bachelor Thesis. Albert-Ludwigs-Universität Freiburg.

Kreissl, S. (2018) Alpine five element veins: reconstruction of a 225 Ma multi-stage Bi-Co-Ni-Fe-As-S system in the Penninic Alps, Switzerland - unraveling compositional, mineralogical and genetic features of five element veins. Petrology and Mineral Resources, Dr. rer. nat. Thesis. Eberhard Karls University, Tübingen, Germany.

Langmuir, D. (1978) Uranium solution-mineral equilibria at low temperatures with applications to sedimentary ore deposits. Geochimica et Cosmochimica Acta, 42(6), 547-569.

Majzlan, J., Drahota, P., and Filippi, M. (2014) Parageneses and crystal chemistry of arsenic minerals. Reviews in Mineralogy and Geochemistry, 79(1), 17-184.

Malinin, S., and Khitarov, N. (1969) Reduction of sulfate sulfur by hydrogen under hydrothermal conditions. Geochemistry International Ussr, 6(6), 1022-1027.
Mandal, B.K., and Suzuki, K.T. (2002) Arsenic round the world: a review. Talanta, 58(1), 201-235.
Markl, G. (2015) Schwarzwald, Vol. 1, Nordschwarzwald and Grube Clara. 672 p. Bode Verlag.
-. (2017) Schwarzwald, Vol. 3, Mittlerer Schwarzwald Teil 2. 640 p.
Markl, G., Burisch, M., and Neumann, U. (2016) Natural fracking and the genesis of five-element veins. Mineralium Deposita, 51(6), 703-712.
Martin, M. (2009) Geogene Grundgehalte (Hintergrundwerte) in den petrogeochemischen Einheiten von Baden-Württemberg. Informationen, p. 98. Landesamt für Geologie, Rohstoffe und Bergbau, Freiburg.
McKinstry, H. (1963) Mineral assemblages in sulfide ores; the system Cu-Fe-As-S. Economic Geology, 58(4), 483-505.
Metz, R., and Richter, M. (1957) Die Blei-Zink-Erzgänge des Schwarzwaldes. 153 p. Amt für Bodenforschung, Hannover.
Migdisov, A.A., and Bychkov, A.Y. (1998) The behaviour of metals and sulphur during the formation of hydrothermal mercury–antimony–arsenic mineralization, Uzon caldera, Kamchatka, Russia. Journal of Volcanology and Geothermal Research, 84(1-2), 153-171.
Mitchell, V.L. (2014) Health risks associated with chronic exposures to arsenic in the environment. Reviews in Mineralogy and geochemistry, 79(1), 435-449.
Muir, T. (1993) The geology of the Hemlo gold deposit area. Ontario Geological Survey, Mines and Minerals Division.
Murzin, V., Naumov, E., Azovskova, O., Varlamov, D., Rovnushkin, M.Y., and Pirajno, F. (2017) The Vorontsovskoe Au-Hg-As ore deposit (Northern Urals, Russia): Geological setting, ore mineralogy, geochemistry, geochronology and genetic model. Ore Geology Reviews, 85, 271-298.
Noble, J.A. (1950) Ore mineralization in the Homestake gold mine, Lead, South Dakota. Geological Society of America Bulletin, 61(3), 221-252.
Nokleberg, W.J. (2005) Metallogenesis and tectonics of the Russian far east, Alaska, and the Canadian cordillera. US Geological Survey.
Nordstrom, D.K. (2002) Worldwide occurrences of arsenic in ground water. Science, 296(5576), 2143-2145.
Nordstrom, D.K., Majzlan, J., and Königsberger, E. (2014) Thermodynamic properties for arsenic minerals and aqueous species. Reviews in Mineralogy and Geochemistry, 79(1), 217-255.
Nordstrom, D.K., and Young, C. (2000) Thermodynamic properties of environmental arsenic species: Limitations and needs. Minor Elements, 325-331.
Ohmoto, H., and Lasaga, A.C. (1982) Kinetics of reactions between aqueous sulfates and sulfides in hydrothermal systems. Geochimica et Cosmochimica Acta, 46(10), 1727-1745.
Ondrus, P., Veselovsky, F., Gabasova, A., Hlousek, J., Srein, V., Vavrin, I., Skala, R., Sejkora, J., and Drabek, M. (2003) Primary minerals of the Jáchymov ore district. Journal of GEOsciences, 48(3-4), 19-146.
Pekov, I.V., Levitskiy, V.V., and Krivovichev, V.G. (2010) Mineralogy of the Belorechenskoye deposit (Northern Caucasus, Russia). Mineralogical Almanac, 15(2), 1-96.
Peters, S.C., Blum, J.D., Karagas, M.R., Chamberlain, C.P., and Sjostrom, D.J. (2006) Sources and exposure of the New Hampshire population to arsenic in public and private drinking water supplies. Chemical Geology, 228(1-3), 72-84.
Pfaff, K., Koenig, A., Wenzel, T., Ridley, I., Hildebrandt, L.H., Leach, D.L., and Markl, G. (2011) Trace and minor element variations and sulfur isotopes in crystalline and colloform ZnS: Incorporation mechanisms and implications for their genesis. Chemical Geology, 286(3-4), 118-134.

Pfaff, K., Romer, R.L., and Markl, G. (2009) U-Pb ages of ferberite, chalcedony, agate,'U-mica'and pitchblende: constraints on the mineralization history of the Schwarzwald ore district. European Journal of Mineralogy, 21(4), 817-836.

Pieczka, A. (2010) Primary Nb-Ta minerals in the Szklary pegmatite, Poland: New insights into controls of crystal chemistry and crystallization sequences. American Mineralogist, 95(10), 1478-1492.

Pierce, M.L., and Moore, C.B. (1982) Adsorption of arsenite and arsenate on amorphous iron hydroxide. Water Research, 16(7), 1247-1253.

Pokrovski, G.S., Borisova, A.Y., and Bychkov, A.Y. (2013) Speciation and transport of metals and metalloids in geological vapors. Reviews in Mineralogy and Geochemistry, 76(1), 165-218.

Powell, W.G., and Pattison, D.R. (1997) An exsolution origin for low-temperature sulfides at the Hemlo gold deposit, Ontario, Canada. Economic Geology, 92(5), 569-577.

Price, R.E., and Pichler, T. (2005) Distribution, speciation and bioavailability of arsenic in a shallow-water submarine hydrothermal system, Tutum Bay, Ambitle Island, PNG. Chemical Geology, 224(1-3), 122-135.

Radosavljević, S.A., Stojanović, J.N., Radosavljević-Mihajlović, A.S., and Vuković, N.S. (2014) Rujevac Sb-Pb-Zn-As polymetallic deposit, Boranja orefield, Western Serbia: native arsenic and arsenic mineralization. Mineralogy and Petrology, 108(1), 111-122.

Reuss, E. (1863) Über die Paragenese der auf den Erzgängen von Příbram einbrechenden Mineralien. Neues Jahrbuch für Mineralogie(65), 13-103.

Robinson, B., and Ohmoto, H. (1973) Mineralogy, fluid inclusions, and stable isotopes of the Echo Bay U-Ni-Ag-Cu deposits, Northwest Territories, Canada. Economic Geology, 68(5), 635-656.

Rye, R.O., and Ohmoto, H. (1974) Sulfur and carbon isotopes and ore genesis: a review. Economic Geology, 69(6), 826-842.

Sakai, H. (1968) Isotopic properties of sulfur compounds in hydrothermal processes. Geochemical Journal, 2(1), 29-49.

Sanjuan, B., Millot, R., Dezayes, C., and Brach, M. (2010) Main characteristics of the deep geothermal brine (5 km) at Soultz-sous-Forêts (France) determined using geochemical and tracer test data. Comptes Rendus Geoscience, 342(7-8), 546-559.

Scharrer, M., Kreissl, S., and Markl, G. (2019) The mineralogical variability of hydrothermal native element-arsenide (five-element) mineralizations and the role of aqueous sulfide. Ore Geology Reviews, 113.

Schürenberg, H. (1950) Die Erzgänge Teufelsgrund und Schindler im Untermünstertal und ihr quantitativer Mineralgehalt.

Schwinn, G., Wagner, T., Baatartsogt, B., and Markl, G. (2006) Quantification of mixing processes in ore-forming hydrothermal systems by combination of stable isotope and fluid inclusion analyses. Geochimica et Cosmochimica Acta, 70(4), 965-982.

Seal, R.R. (2006) Sulfur isotope geochemistry of sulfide minerals. Reviews in mineralogy and geochemistry, 61(1), 633-677.

Sergeyeva, E., and Khodakovskiy, I. (1969) Physicochemical conditions of formation of native arsenic in hydrothermal deposits. Geokhimiya(7), 846-859.

Sharp, J.O., Lezama-Pacheco, J.S., Schofield, E.J., Junier, P., Ulrich, K.-U., Chinni, S., Veeramani, H., Margot-Roquier, C., Webb, S.M., and Tebo, B.M. (2011) Uranium speciation and stability after reductive immobilization in aquifer sediments. Geochimica et Cosmochimica Acta, 75(21), 6497-6510.

Shcherbina, V.V. (1978) Chemical reactions in natural sulfide systems. Geokhimiya(9), 1283-1291.

Staude, S., Bons, P.D., and Markl, G. (2009) Hydrothermal vein formation by extension-driven dewatering of the middle crust: An example from SW Germany. Earth and Planetary Science Letters, 286(3-4), 387-395.

Staude, S., Werner, W., Mordhorst, T., Wemmer, K., Jacob, D.E., and Markl, G. (2012) Multi-stage Ag–Bi–Co–Ni–U and Cu–Bi vein mineralization at Wittichen, Schwarzwald, SW Germany: geological setting, ore mineralogy, and fluid evolution. Mineralium Deposita, 47(3), 251-276.

Su, W., Heinrich, C.A., Pettke, T., Zhang, X., Hu, R., and Xia, B. (2009) Sediment-hosted gold deposits in Guizhou, China: products of wall-rock sulfidation by deep crustal fluids. Economic Geology, 104(1), 73-93.

Taylor, C.M., and Radtke, A.S. (1969) Micromineralogy of silver-bearing sphalerite from Flat river, Missouri. Economic Geology, 64(3), 306-318.

Tomkins, A.G., Pattison, D.R., and Zaleski, E. (2004) The Hemlo gold deposit, Ontario: An example of melting and mobilization of a precious metal-sulfosalt assemblage during amphibolite facies metamorphism and deformation. Economic Geology, 99(6), 1063-1084.

Vochten, R., and Goeminne, A. (1984) Synthesis, crystallographic data, solubility and electrokinetic properties of meta-zeunerite, meta-kirchheimerite and nickel-uranylarsenate. Physics and Chemistry of Minerals, 11(2), 95-100.

Vokes, F.M. (1963) Geological studies on the Caledonian pyritic zinc-lead orebody at Bleikvassli, Norland, Norway. Universitetsforlaget.

Voudouris, P., Melfos, V., Spry, P., Bonsall, T., Tarkian, M., and Economou-Eliopoulos, M. (2008) Mineralogical and fluid inclusion constraints on the evolution of the Plaka intrusion-related ore system, Lavrion, Greece. Mineralogy and Petrology, 93(1-2), 79-110.

Walenta, K., and Wimmenauer, W. (1961) Der Mineralbestand des Michaelganges im Weiler bei Lahr (Schwarzwald). Jahreshefte des Geologischen Landesamts in Baden-Wuerttemberg, 4, 7-37.

Walter, B.F., Burisch, M., Fusswinkel, T., Marks, M.A., Steele-MacInnis, M., Wälle, M., Apukhtina, O.B., and Markl, G. (2018) Multi-reservoir fluid mixing processes in rift-related hydrothermal veins, Schwarzwald, SW-Germany. Journal of Geochemical Exploration, 186, 158-186.

Walter, B.F., Burisch, M., and Markl, G. (2016) Long-term chemical evolution and modification of continental basement brines–a field study from the Schwarzwald, SW Germany. Geofluids, 16(3), 604-623.

Walter, B.F., Burisch, M., Marks, M.A., and Markl, G. (2017) Major element compositions of fluid inclusions from hydrothermal vein-type deposits record eroded sedimentary units in the Schwarzwald district, SW Germany. Mineralium Deposita, 52(8), 1191-1204.

Wilkinson, J.J., Eyre, S.L., and Boyce, A.J. (2005) Ore-forming processes in Irish-type carbonate-hosted Zn-Pb deposits: Evidence from mineralogy, chemistry, and isotopic composition of sulfides at the Lisheen Mine. Economic Geology, 100(1), 63-86.

Woitsekhowskaya, M., and Peters, S. (1998) Geochemical modeling of alteration and gold deposition in the Betze deposit, Eureka County, Nevada. Contributions to the gold metallogeny of northern Nevada: US Geological Survey Open-File Report 98, p. 211-222.

Wu, Y., Zhou, X.-y., Lei, M., Yang, J., Ma, J., Qiao, P.-w., and Chen, T.-b. (2017) Migration and transformation of arsenic: contamination control and remediation in realgar mining areas. Applied Geochemistry, 77, 44-51.

Zheng, B., Zhu, Y., An, F., Huang, Q.-y., and Qiu, T. (2015) As–Sb–Bi–Au mineralization in the Baogutu gold deposit, Xinjiang, NW China. Ore Geology Reviews, 69, 17-32.

Zhu, Y., An, F., and Tan, J. (2011) Geochemistry of hydrothermal gold deposits: a review. Geoscience Frontiers, 2(3), 367-374.

Table Footnotes

1. Compilation of mineralizations that are nat. As bearing. Mineral abbreviations: asp = arsenopyrite, gn = galena, nat. As = native arsenic, nat. Bi = native bismuth, orp = orpiment, py = pyrite, rg = realgar, sbn = stibnite, sph = sphalerite,

2. Thermodynamic data ($\Delta_f G$ in kJ/mol) estimated or selected and incorporated into the preexisting thermodynamic databases used in this study. [1] represents Vochten and Goeminne (1984)

3. Compilation of minerals discussed in this manuscript.

4. Representative EPMA analyses.

Figure captions

Figure 1. Geological map and cross-section presenting the horst-graben type structural control of the mineralization of the Michael vein.

Figure 2. (**a**) Generalized paragenetic sequence of important ore, gangue and supergene minerals. (**b**) Detailed mineralogical sequence of ore stage IIa with respect to the two texturally occurring types.

Figure 3. Images of hand specimen that depict the typical occurrence of stage I (**a**) and stage II (**b**-**d**). (**b**) Characteristic brecciation of the vein and subsequent cementing by stage II minerals, in this case arsenic. The Zn-sulfides occur as either colloform textured aggregates of sphalerite and wurzite (**c**) or as aggregates of sub- to euhedral crystals of sphalerite (**d**).

Figure 4. Pyrite (**a**) and graphite (**b**) are enclosed in sphalerite. Jordanite-gratonite solid solution minerals formed prior to/ during sphalerite precipitation (**c**,**d**). Galena can also be found as small grains in individual nat. As bands (**e**), but typically forms before/ during the initiation of nat. As, and is thus found as inclusions in nat. As (**f**). The triarsenide, skutterudide is rather rare and mostly occurs at the transition between sphalerite and nat. As formation (**g**). Mineral aggregates are characteristically brecciated and cemented by subsequent minerals, where jordanite crystals are commonly pseudomorphed by nat. As (**h**,**i**). (**c**,**gh**, **i**) represent colloform samples and (**a**,**b**,**d**,**e**,**f**) represent non-colloform samples. Image types: (**c**) BSE image, (**a**,**b**,**d-h**) reflected light and (**h**,**i**) slightly dejusted but crossed polarized reflected light.

959 **Figure 5.** Ore stage IIa minerals are commonly brecciated and cemented by fine grained quartz
960 (**a**), partially dissolved (**b**) or replaced (**c**). (**d**) A rare second generation of nat. As can form
961 remarkable overgrowths on realgar crystals. (**e**,**f**) Supergene druse fillings sometimes incorporate
962 uranyl arsenates. Image types: (**a**) reflected light, (**b**,**c**) crossed polarized reflected light and
963 (**d**,**e**,**f**) hand specimen images.

964

965 **Figure 6.** Compositional analyses of Zn-sulfides, classified according to their textural
966 occurrence, plotted to visualize potential micro-intergrowth with other minerals. Mineral
967 abbreviations: chalcopyrite (cp), fahlore (fhl), galena (gn), gersdorffite (gdf), jordanite-gratonite
968 solid-solution (jdn-gtn) and skutterudite (skut).

969

970 **Figure 7.** *pH-logf*O_2 diagrams depicting mineral stabilities. Note stabilities may overlap, e.g., at
971 the stability conditions of galena, sphalerite is also stable. Diagrams (**a**,**b**) show the
972 thermodynamic stability of the Michael vein mineralogy at roughly neutral conditions. (**c**,**d**)
973 Striped-shaded region in represents the stability fields of As-sulfides, sphalerite, galena and
974 jordanite and is identical to (**a**). The bottom diagrams (**c**,**d**) show the impact of even slight
975 amounts of Ni or Fe on the stability of Ni- and Fe-minerals.

976

977 **Figure 8.** (**a**) Qualitative formation model of the Michael vein, nat. As-base metal mineralization.
978 (**b**) Qualitative diagrams depicting the impact of abundant Zn in stabilizing nat. As at higher
979 sulfidation states.

980

Figure 9. *pH-logfO_2* diagrams depicting mineral stabilities at higher Fe concentrations. Note stabilities may overlap, e.g., at the stability conditions of galena, sphalerite is also stable. The stability of arsenopyrite suppresses the stability of nat. As and thus preventing it from forming at a neutral pH, even at reduced conditions.

Figure 10. *Temp.-logfO_2* diagram at neutral conditions showing the impact of temperature on the stabilities of the minerals from the Michael vein. Fluid conditions are identical to Fig. 7a.

Figure 11. *As-* and *S- logfO_2* diagrams depicting the impact of variable As and S content on the stability of the minerals from the Michael vein at neutral conditions. Both, As and S increase the stability of the As-sulfides. Thus, to form nat. As from a fluid with abundant As, sulfide must be absent.

Figure 12. (**a**) Qualitative formation model for the uranyl arsenates presented by the example of the Pb-uranyl arsenates hügelite and hallimondite. Fluid-mineral reaction stability diagrams for (**b**) an arsenic-bearing fluid reacting with galena in the presence of various amounts of phosphor, (**c**) and the stability of Pb-arsenate, uranylarsenate and sulfate in the presence of various amount of chlorine (d) an arsenic-bearing fluid reacting with galena in the presence of various amounts of chalcopyrite. The uncertainty introduced by estimation of the solubility estimation of hallimondite is given by the striped area and dashed lines. The diagrams show that even at low U content of the fluid, uranyl arsenates can form. Furthermore, the Cu-uranyl arsenates are significantly more stable than the predicted Pb-uranyl arsenates.

This is a preprint, the final version is subject to change, of the American Mineralogist (MSA)
Cite as Authors (Year) Title. American Mineralogist, in press.
DOI: https://doi.org/10.2138/am-2020-7062

1003

1004

This is a preprint, the final version is subject to change, of the American Mineralogist (MSA)
Cite as Authors (Year) Title. American Mineralogist, in press.
DOI: https://doi.org/10.2138/am-2020-7062

mineralization type	examples	major ore minerals	major arsenic mineral (with sequence)	nat. As abundance	formation mechanism of the mineralization	Temp [°C]	sal [NaCl eq. Wt %]	fluid composition of As paragenesis	
Sediment hosted replacement (Carlin-type) gold deposits	Guizhou, China Betze, USA Vorontsovskoe, Russia	asp, py	asp, (nat. As) → rg, orp (after py formation)	-	sulfidation of the host rock (and reduction of the fluid)	150-220		ca. 50-350 mg/kg As, Fe is b.d.l.	Kesler et al. 2005, Su et al. 2009, Woitsekhowskaya & Peters 2015, Murzin et al. 2017
vein-type Orogenic/ magmatic gold deposits	Baia Mare, Romania Baogutu, China	asp, py, sbn	asp → nat. As (after py formation)	-	fluid cooling	150-300	0-5		Bailly et al. 1998, Grancea et al. 2002, Zheng et al. 2015
nat. element-arsenide ("five-element")	Erzgebirge, Germany Schwarzwald, Germany Odenwald, Germany	arsenides, nat. Ag, nat. Bi	arsenides → nat. As	++	reduction	100-500	0-50		Markl et al 2016, Scharrer et al. in review, Burisch et al 2017
epithermal ore shoots in base metal veins	Schwarzwald, Germany	gn, sph	nat. As, arsenides	0					Schürenberg 1950, Metz et al. 1957
polymetallic veins	Rujevac, Serbia Schwarzwald, Germany	gn, sph, py, Pb-sulfosalts	asp/py → nat. As → rg, orp	0		100-230			Radosavljević et al. 2014, this study
stratabound As mineralizations in fractured Karbonates	Saualpe, Austria Binntal, Switzerland	rg, nat. As	rg, orp → nat. As	+					Göd & Zemann 2000, Hofmann & Knill 1996
fracture controlled As-mineralization in rhyolitic rocks	Sailauf, Germany	nat. As	nat. As	+					Fusswinkel et al. 2014
disseminated ore in pegmatites	Bernic lake, Canada	nat. Bi, gn, stibarsen, nat. As	nat. As, stibarsen	-		<300			Cerny & Harris 1978, Pieczka 2010
active geothermal fields (hotsprings)	Uzon, Russia	sbn, rg, orp	nat. As → rg → orp, (alacranite, uzonite)	0	boiling, cooling and mixing	75-85		pH 3-6, ca 130 mg/l S, 0.2-9 mg/l As	Migdisov & Bychkov 1998; Cleverley et al. 2003
metamorphosed Au deposit	Hemlo Au-deposit, Canada		nat. As, rg, orp	-	exolution from metamorpic solid solution	<600			Tomkins et al 2014, Muir 1993, Powell & Pattison 1997
coal combustion	Kladno, Czech Republic St. Etiene, France		nat. As, rg, orp	+					Majzlan et al 2014

This is a preprint, the final version is subject to change, of the American Mineralogist (MSA)
Cite as Authors (Year) Title. American Mineralogist, in press.
DOI: https://doi.org/10.2138/am-2020-7062

	0 °C	25 °C	60 °C	100 °C	150 °C	200 °C	250 °C	300 °C	source
Pb14As6S23	-1670	-1679	-1693	-1710	-1736	-1765	-1798	-1834	estimated
Pb2UO2(AsO4)2:2H2O	-3012±15								estimated
Cu(UO2)2(AsO4)2*8H2O	-5315								[1]

Mineral	Formula
sulfosalts, sulfarsenides and arsenides	
chalcopyrite	$CuFeS_2$
galena	PbS
gersdorffite	$NiAsS$
gratonite	$Pb_9As_4S_{15}$
jordanite-geocronite	$Pb_{14}(As,Sb)_6S_{23}$
orpiment	As_2S_3
pyrite	FeS_2
realgar	As_4S_4
skutterudite	$(Ni,Co,Fe)As_3$
sphalerite/ wurzite	ZnS
tennantite	$Cu_6[Cu_4(Fe,Zn)_2]As_4S_{13}$
native elements:	
graphite	C
native arsenic	As
supergene minerals	
adamite	Zn_2AsO_4OH
anglesite	$PbSO_4$
cerussite	$PbCO_3$
goethite	$FeO(OH)$
hallimondite	$Pb_2(UO_2)(AsO_4)_2 \cdot 2H_2O$
heinrichite	$Ba(UO_2)_2(AsO_4)_2 \cdot 8\text{-}10H_2O$
hügelit	$Pb_2(UO_2)_3(AsO_4)_2O_2 \cdot 5H_2O$
malachite	$Cu_2CO_3(OH)_2$
meta-zeunerite	$Cu(UO_2)_2(AsO_4)_2 \cdot 8H_2O$
mimetite	$Pb_5(AsO_4)_3Cl$
parsonsite	$Pb_2(UO_2)(PO_4)_2 \cdot 2H_2O$

This is a preprint, the final version is subject to change, of the American Mineralogist (MSA)
Cite as Authors (Year) Title. American Mineralogist, in press.
DOI: https://doi.org/10.2138/am-2020-7062

mineral	pyrite	sphalerite coll.	sphalerite coll.	sphalerite non-coll.	sphalerite non-coll.	jordanite	jordanite	galena	fahlore	chalco-pyrite	skutteru-dite	nat. arsenic	nat. arsenic	para-realgar
sample	LK11	BW95	BW95	KS8	LK11	1376	LK2	KS5a	Fhl	L4	L4	BW100	LK2	BW102
EPMA analysis [wt%]														
Mn		b.d.l.	b.d.l.	0,011	b.d.l.									
Fe	46,390	0,047	0,247	0,034	0,909	0,011	0,044	0,043	1,340	30,127	5,195	b.d.l.	0,009	b.d.l.
Co	b.d.l.					b.d.l.	b.d.l.	b.d.l.	b.d.l.	b.d.l.	3,444	b.d.l.	b.d.l.	b.d.l.
Ni	b.d.l.					b.d.l.	b.d.l.	b.d.l.	b.d.l.	b.d.l.	12,618	b.d.l.	b.d.l.	b.d.l.
Cu	b.d.l.	b.d.l.	b.d.l.	b.d.l.	b.d.l.	b.d.l.	b.d.l.	b.d.l.	42,807	33,102	b.d.l.	b.d.l.	b.d.l.	b.d.l.
Ag	b.d.l.	b.d.l.	b.d.l.	b.d.l.	b.d.l.	b.d.l.	b.d.l.	0,035	b.d.l.	b.d.l.	b.d.l.	b.d.l.	b.d.l.	b.d.l.
Cd		0,401	b.d.l.	b.d.l.	b.d.l.									
Zn	b.d.l.	65,781	64,905	66,693	66,127	0,140	0,253	0,019	6,859	b.d.l.	b.d.l.	b.d.l.	0,167	0,017
Pb	b.d.l.	0,299	1,311	0,041	b.d.l.	67,596	69,355	86,274	b.d.l.	b.d.l.	b.d.l.	b.d.l.	0,132	b.d.l.
Se	b.d.l.					0,018	0,031	b.d.l.	b.d.l.	b.d.l.	b.d.l.	0,578	0,597	0,180
Hg	b.d.l.					0,083	b.d.l.	b.d.l.	b.d.l.	b.d.l.	b.d.l.	b.d.l.	b.d.l.	b.d.l.
S	53,779	32,696	32,397	33,193	32,768	17,103	17,933	13,561	28,710	35,002	5,520	0,341	0,446	29,036
Bi	b.d.l.					b.d.l.	b.d.l.	b.d.l.	b.d.l.	b.d.l.	b.d.l.	b.d.l.	b.d.l.	b.d.l.
As	0,137	0,128	0,205	0,035	0,066	5,223	8,226	0,074	19,534	0,173	73,529	98,134	98,691	70,655
Sb	b.d.l.	0,187	0,424	b.d.l.	b.d.l.	8,144	4,154	b.d.l.	0,830	b.d.l.	b.d.l.	0,354	0,253	0,266
∑	100,31	99,61	99,58	100,01	99,87	98,32	100,00	100,01	100,08	98,40	100,31	99,41	100,30	100,15
empirical formula	$Fe_{0.99}S_{2.00}$	$Zn_{1.00}S_{1.00}$	$Zn_{0.99}Pb_{0.01}S_{1.00}$	$Zn_{0.99}S_{1.01}$	$Zn_{1.00}S_{1.00}$	$Fe_{0.01}Zn_{0.09}Pb_{14.14}Se_{0.01}Hg_{0.01}S_{22.95}As_{3.00}Sb_{2.88}$	$Fe_{0.03}Zn_{0.16}Pb_{13.80}Se_{0.02}S_{23.06}As_{4.53}Sb_{1.41}$	$Pb_{1.00}S_{1.00}$	$Cu_{9.94}Fe_{0.35}Zn_{1.55}S_{13.21}As_{3.85}Sb_{0.10}$	$Cu_{0.97}Fe_{1.00}S_{2.03}$	$Ni_{0.57}Co_{0.15}Fe_{0.24}As_{2.58}S_{0.45}$			$As_{1.02}S_{0.98}$

	mimetite	mimetite
	KS1	KS3
PbO	78.831	74.931
CaO	b.d.l.	b.d.l.
BaO	b.d.l.	b.d.l.
ZnO	b.d.l.	b.d.l.
CuO	b.d.l.	b.d.l.
FeO	b.d.l.	b.d.l.
SiO_2	b.d.l.	b.d.l.
SO_2	b.d.l.	b.d.l.
P_2O_5	6.439	b.d.l.
As_2O_5	14.173	23.499
V_2O_3	b.d.l.	b.d.l.
UO_2	b.d.l.	0.812
Cl	2.37	2.02
F	b.d.l.	b.d.l.
empirical formula	$Pb_{5.01}P_{1.29}As_{1.75}O_{12}Cl_{0.95}$	$Pb_{5.01}U_{0.05}P_{1.29}As_{1.75}O_{12}Cl_{0.95}$

Figure 1

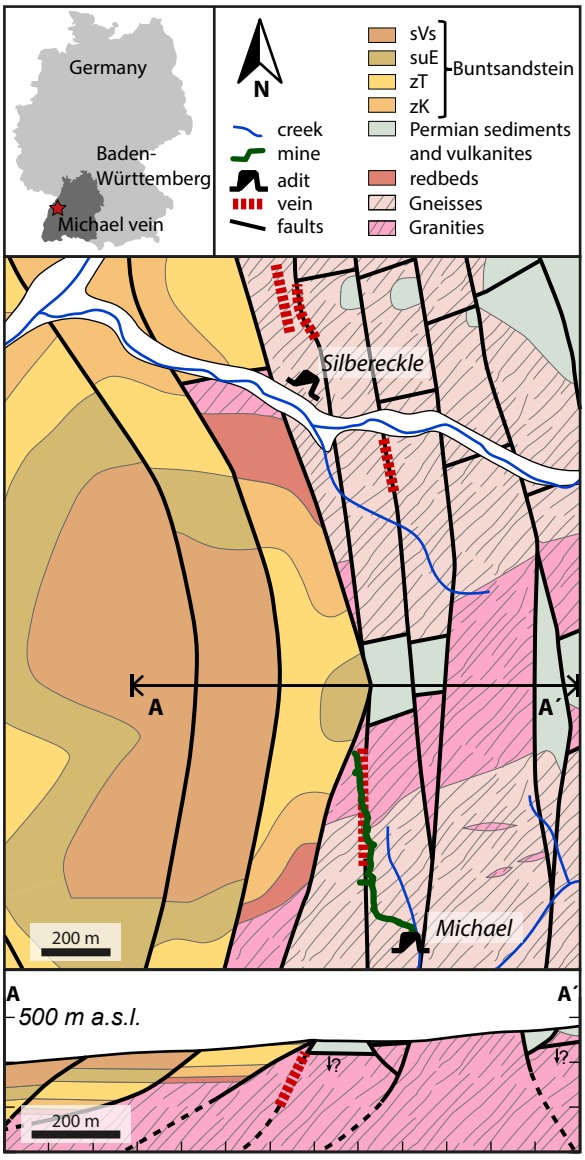
Germany
Baden-
Württemberg
Michael vein
N
creek
mine
adit
vein
faults
sVs
suE
zT
zK
Buntsandstein
Permian sediments
and vulkanites
redbeds
Gneisses
Granities
Silbereckle
A
A´
Michael
200 m
A
A´
500 m a.s.l.
200 m

Figure 2

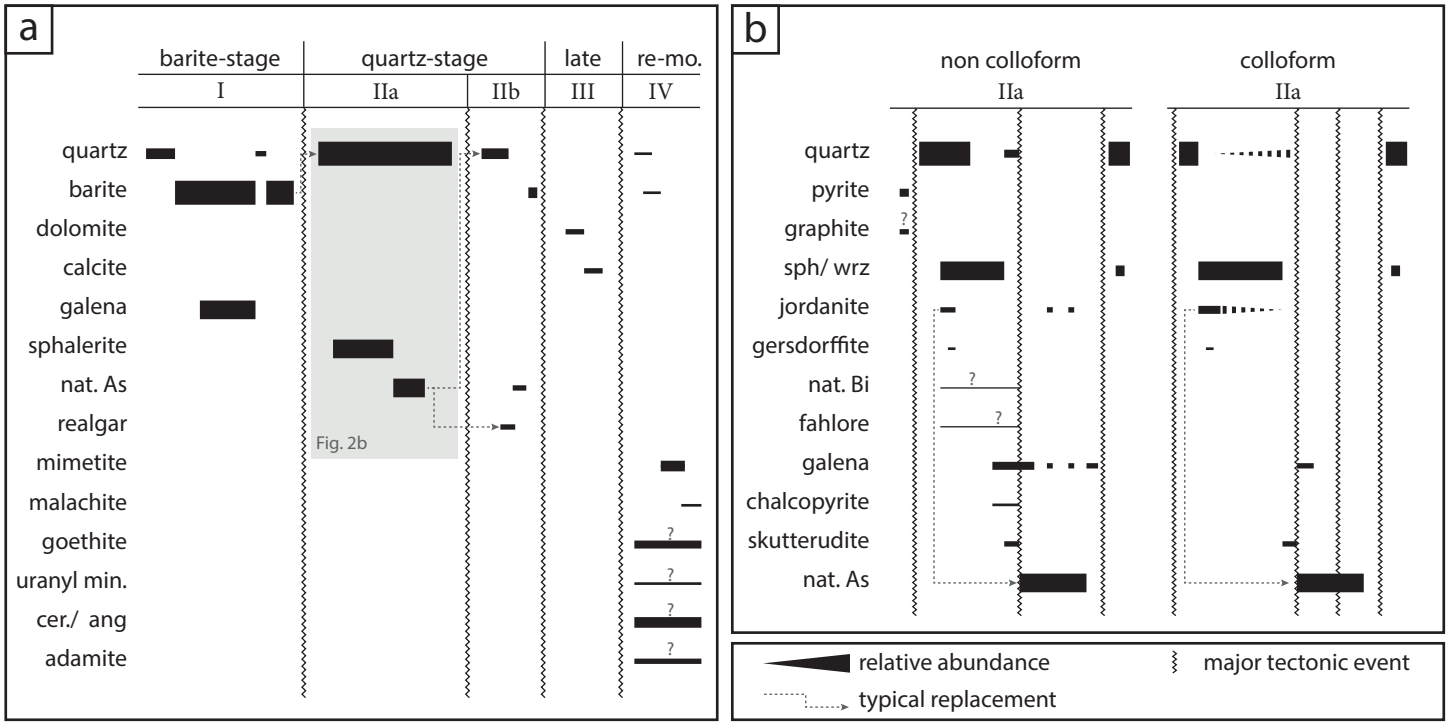
a
barite-stage
quartz-stage
late
re-mo.
I
IIa
IIb
III
IV
quartz
barite
dolomite
calcite
galena
sphalerite
nat. As
realgar
mimetite
malachite
goethite
uranyl min.
cer./ ang
adamite
Fig. 2b
b
non colloform
colloform
IIa
IIa
quartz
pyrite
graphite
sph/ wrz
jordanite
gersdorffite
nat. Bi
fahlore
galena
chalcopyrite
skutterudite
nat. As
relative abundance
major tectonic event
typical replacement

Figure 3

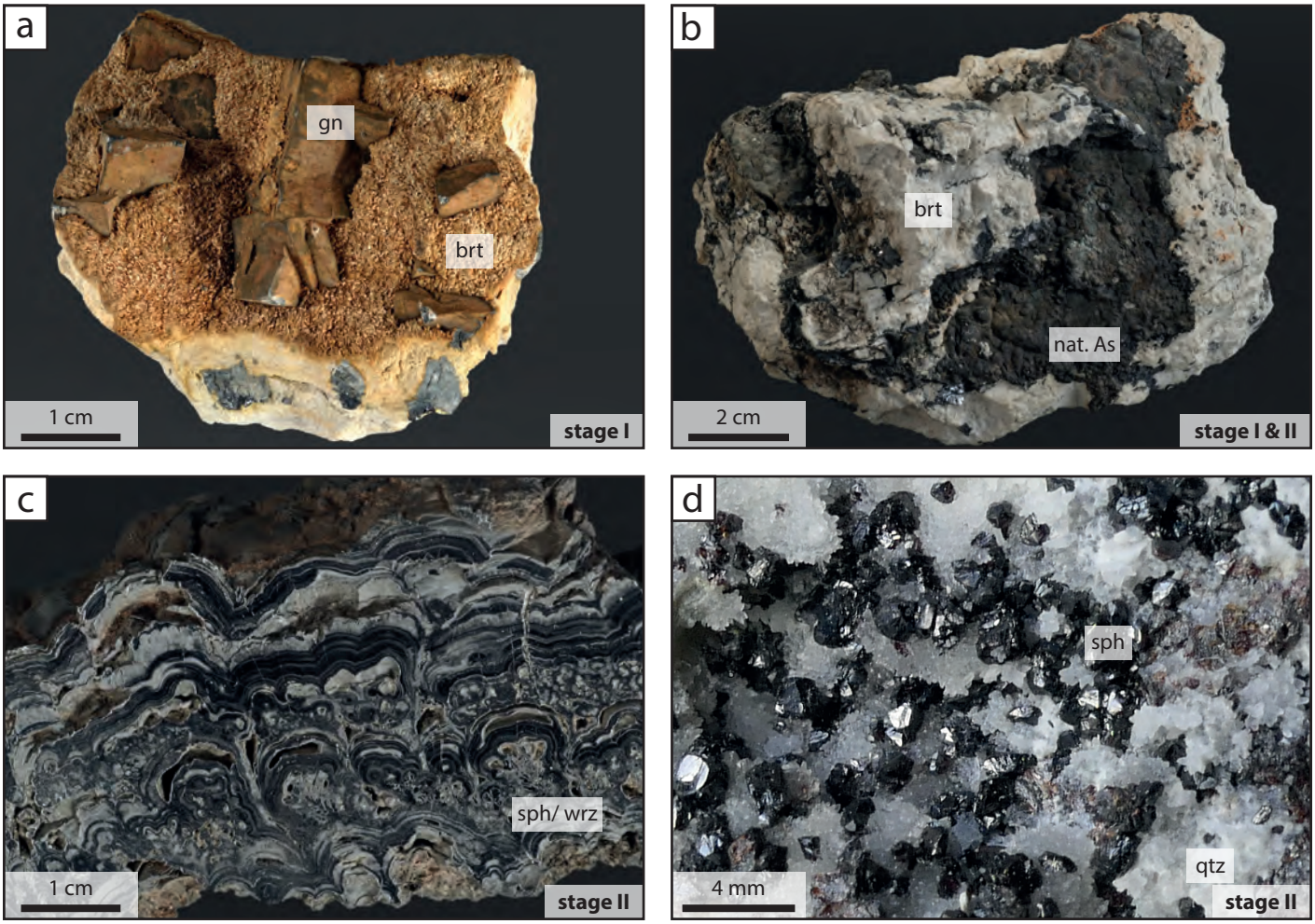
a
gn
brt
1 cm
stage I
b
brt
nat. As
2 cm
stage I & II
c
sph/ wrz
1 cm
stage II
d
sph
qtz
4 mm
stage II

Figure 4

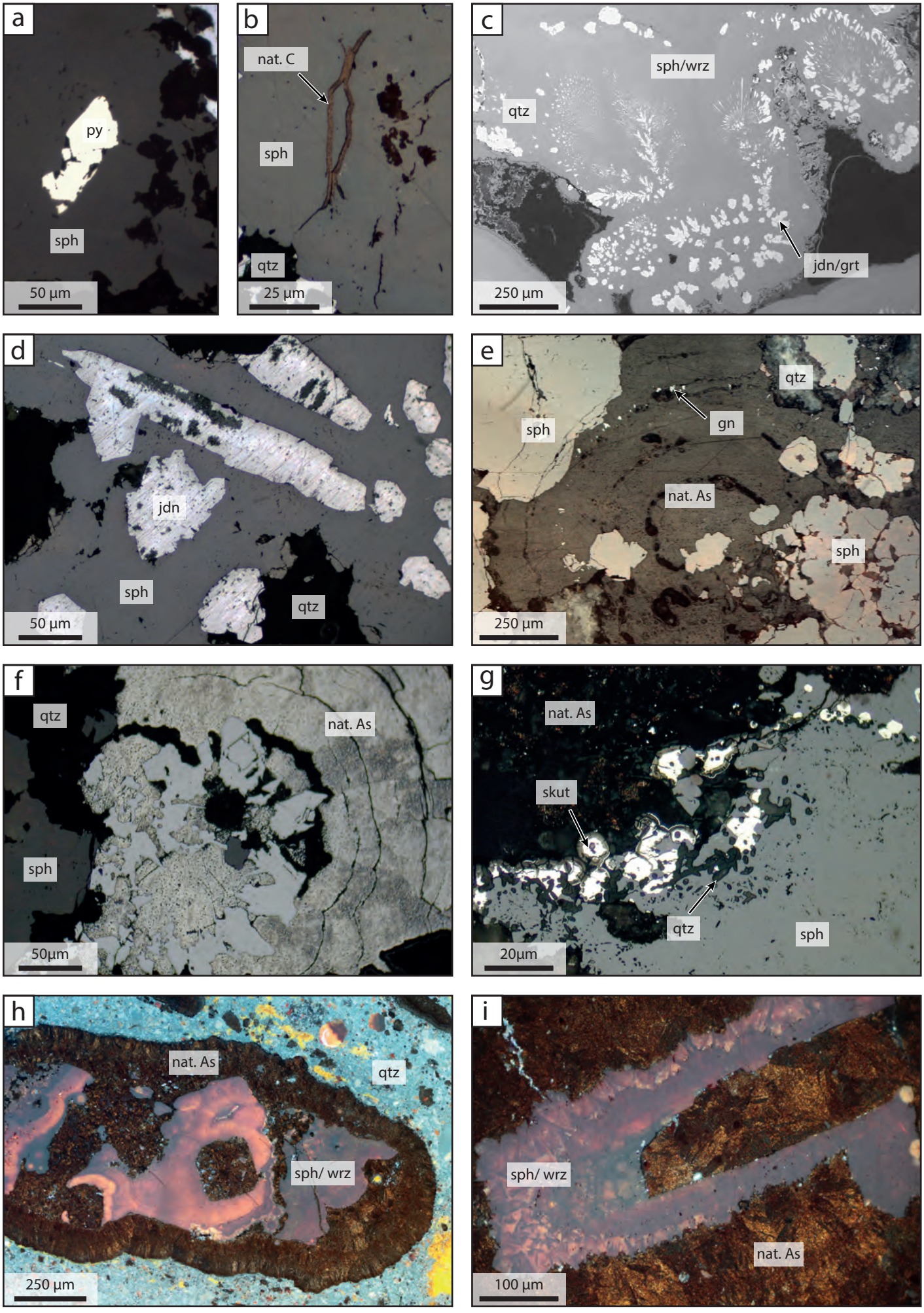
a
py
sph
50 µm
b
nat. C
sph
qtz
25 µm
c
sph/wrz
qtz
jdn/grt
250 µm
d
jdn
sph
qtz
50 µm
e
qtz
gn
sph
nat. As
sph
250 µm
f
qtz
nat. As
sph
50µm
g
nat. As
skut
qtz
sph
20µm
h
nat. As
qtz
sph/ wrz
250 µm
i
sph/ wrz
nat. As
100 µm

Figure 5

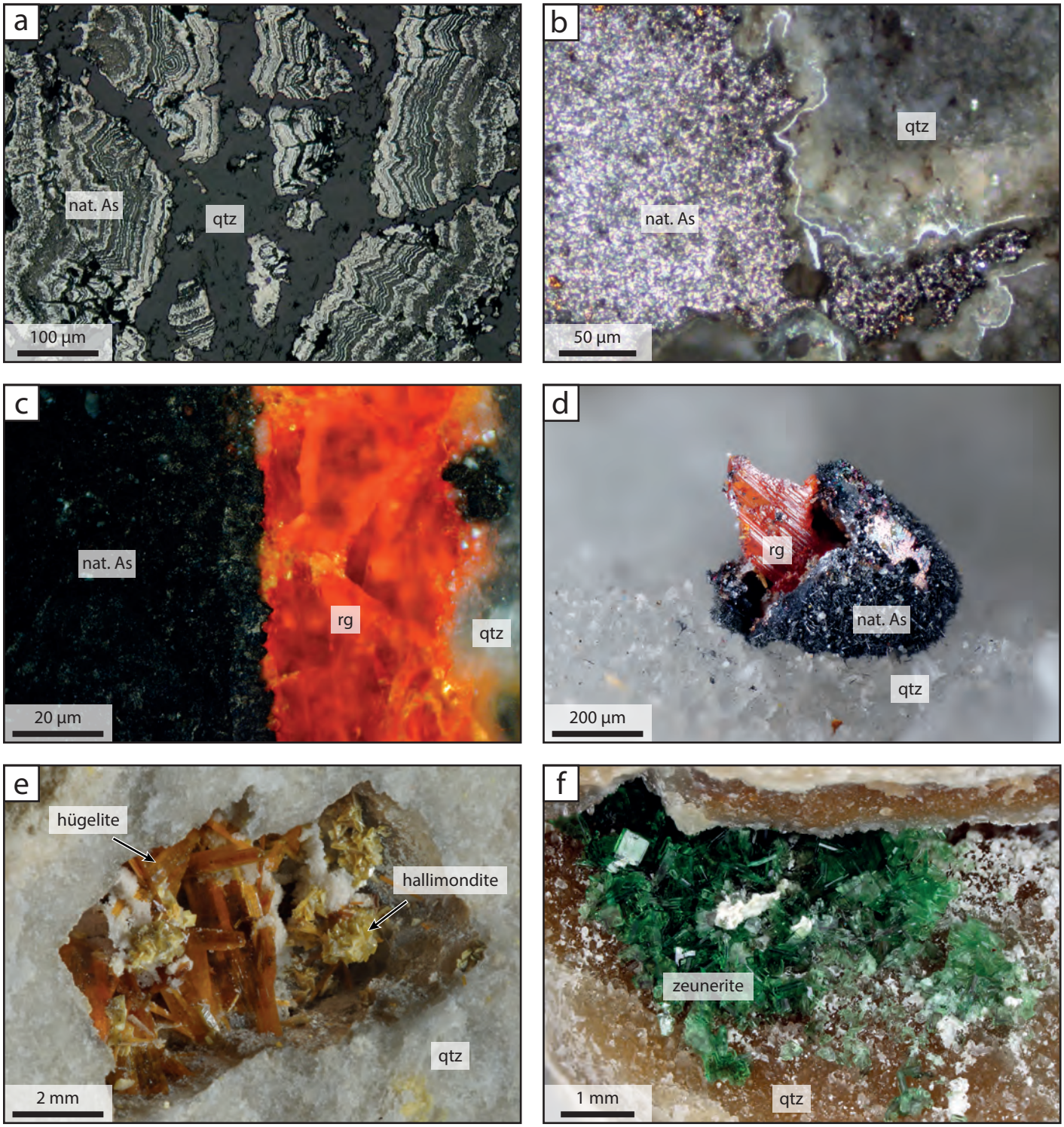
a
nat. As
qtz
100 µm
b
qtz
nat. As
50 µm
c
nat. As
rg
qtz
20 µm
d
rg
nat. As
qtz
200 µm
e
hügelite
hallimondite
qtz
2 mm
f
zeunerite
qtz
1 mm

Figure 6

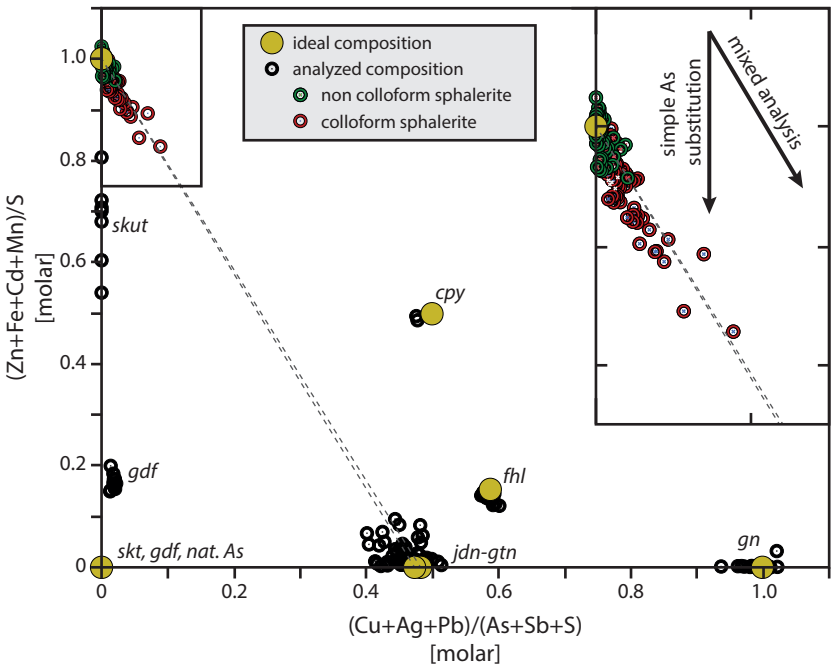
ideal composition
analyzed composition
non colloform sphalerite
colloform sphalerite
simple As substitution
mixed analysis
skut
cpy
gdf
fhl
skt, gdf, nat. As
jdn-gtn
gn
(Zn+Fe+Cd+Mn)/S [molar]
(Cu+Ag+Pb)/(As+Sb+S) [molar]
0
0.2
0.4
0.6
0.8
1.0

Figure 7

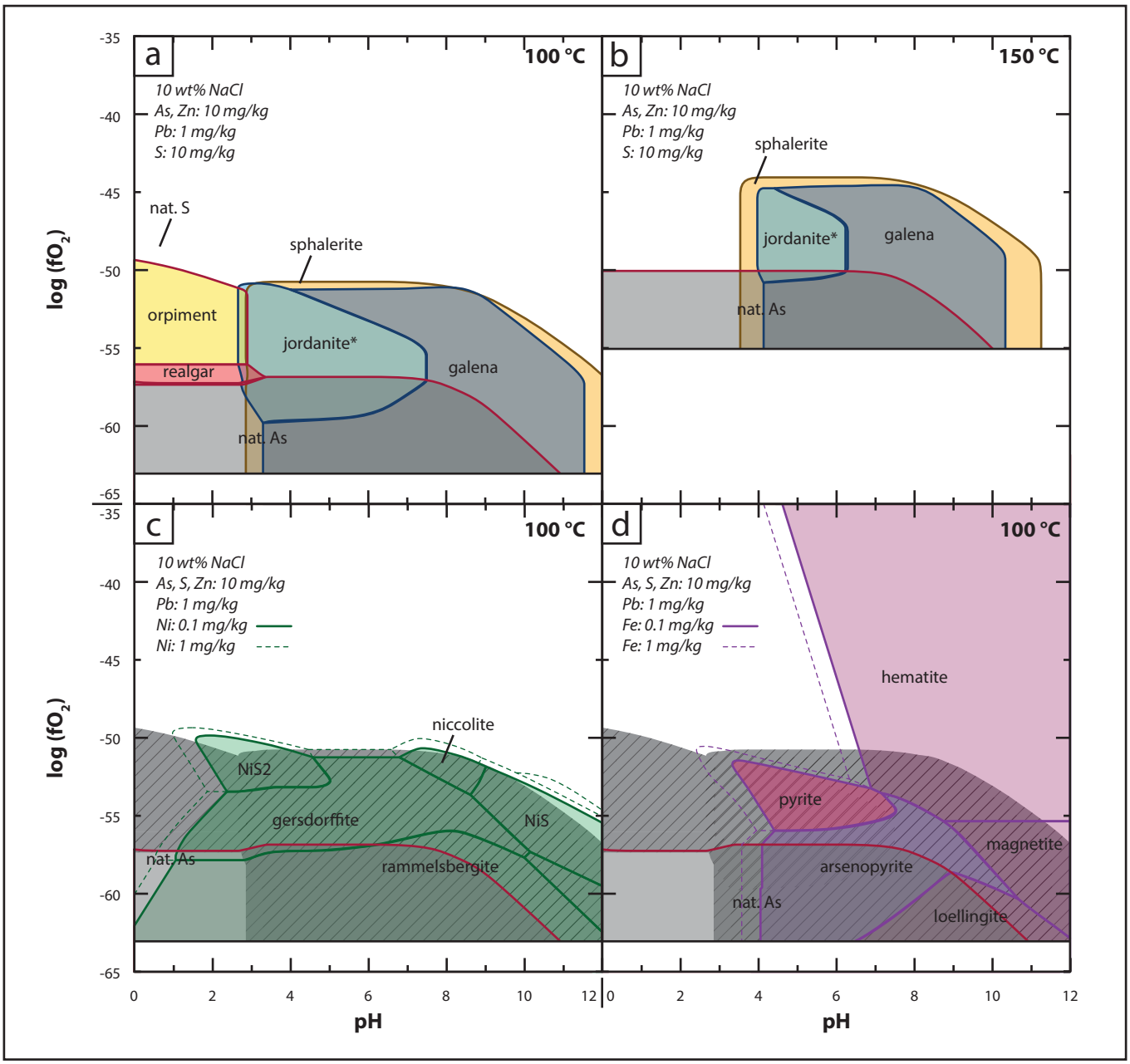
a
100 °C
10 wt% NaCl
As, Zn: 10 mg/kg
Pb: 1 mg/kg
S: 10 mg/kg
nat. S
sphalerite
orpiment
jordanite*
realgar
galena
nat. As
b
150 °C
10 wt% NaCl
As, Zn: 10 mg/kg
Pb: 1 mg/kg
S: 10 mg/kg
sphalerite
jordanite*
galena
nat. As
c
100 °C
10 wt% NaCl
As, S, Zn: 10 mg/kg
Pb: 1 mg/kg
Ni: 0.1 mg/kg
Ni: 1 mg/kg
niccolite
NiS2
gersdorffite
NiS
nat. As
rammelsbergite
d
100 °C
10 wt% NaCl
As, S, Zn: 10 mg/kg
Pb: 1 mg/kg
Fe: 0.1 mg/kg
Fe: 1 mg/kg
hematite
pyrite
magnetite
arsenopyrite
nat. As
loellingite
log (fO2)
pH
-35
-40
-45
-50
-55
-60
-65
0
2
4
6
8
10
12

Figure 8

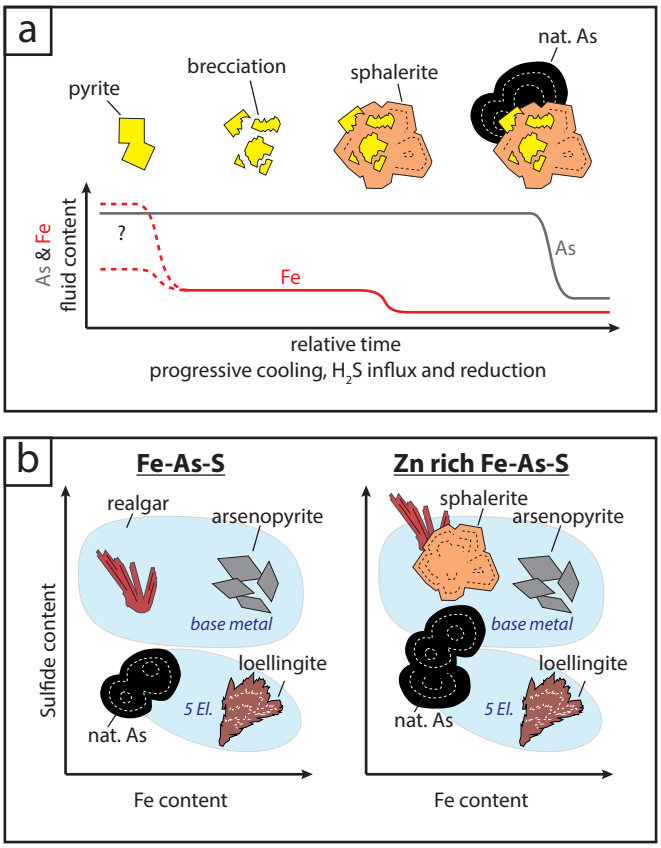
a
pyrite
brecciation
sphalerite
nat. As
As & Fe fluid content
?
Fe
As
relative time
progressive cooling, H2S influx and reduction
b
Fe-As-S
Zn rich Fe-As-S
realgar
arsenopyrite
base metal
loellingite
5 El.
nat. As
sphalerite
Sulfide content
Fe content

Figure 9

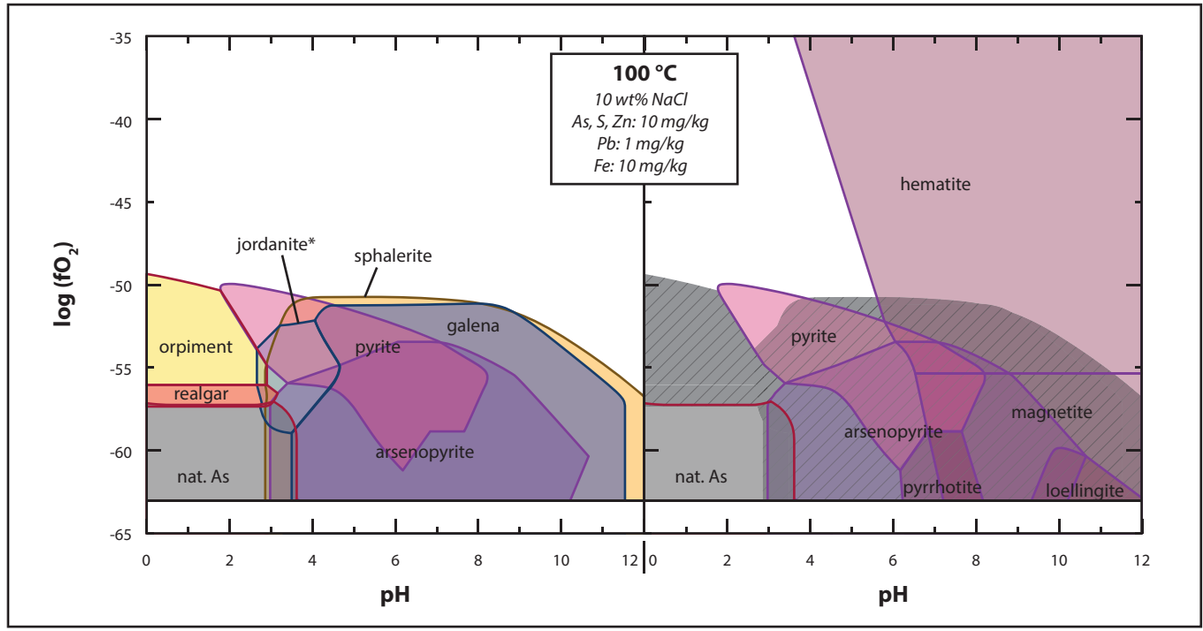
100 °C
10 wt% NaCl
As, S, Zn: 10 mg/kg
Pb: 1 mg/kg
Fe: 10 mg/kg
log (fO2)
-35
-40
-45
-50
-55
-60
-65
0
2
4
6
8
10
12
pH
jordanite*
sphalerite
orpiment
realgar
nat. As
pyrite
galena
arsenopyrite
hematite
pyrite
arsenopyrite
magnetite
pyrrhotite
loellingite
nat. As

Figure 10

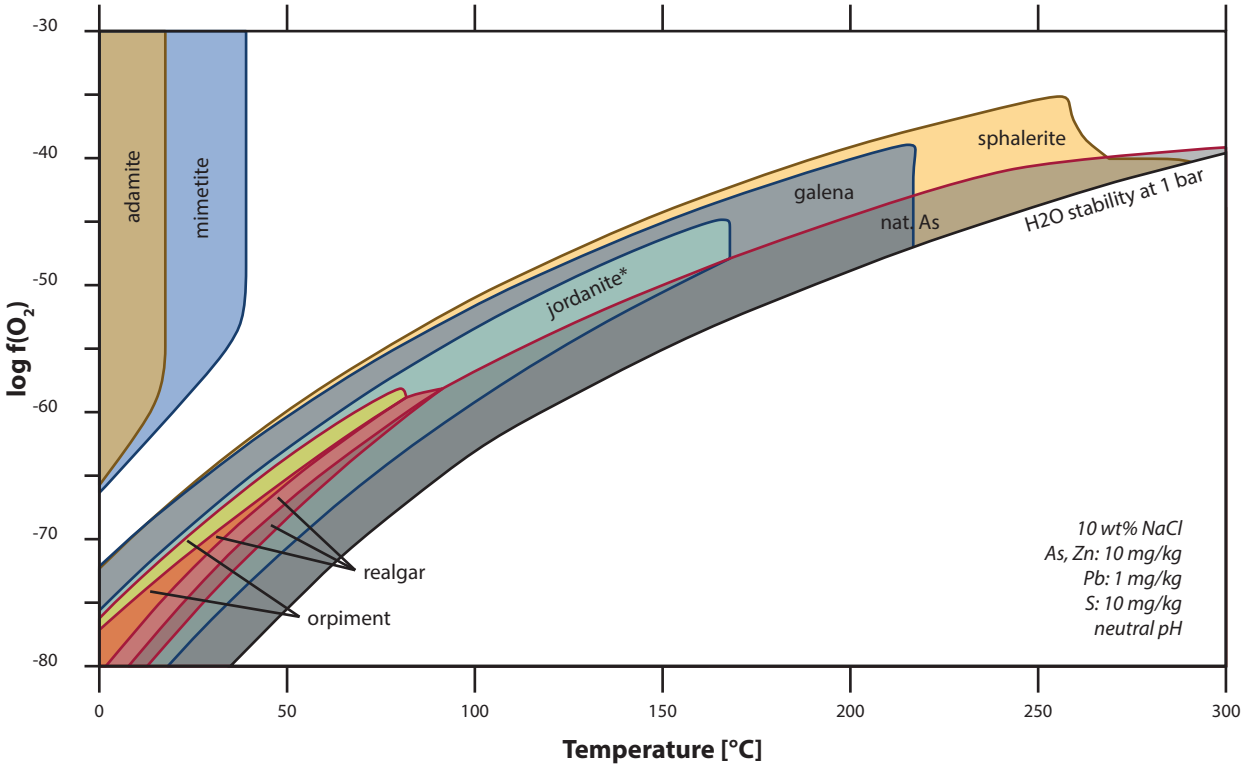
-30
-40
-50
-60
-70
-80
log f(O2)
0
50
100
150
200
250
300
Temperature [°C]
adamite
mimetite
sphalerite
galena
nat. As
H2O stability at 1 bar
jordanite*
realgar
orpiment
10 wt% NaCl
As, Zn: 10 mg/kg
Pb: 1 mg/kg
S: 10 mg/kg
neutral pH

Figure 11

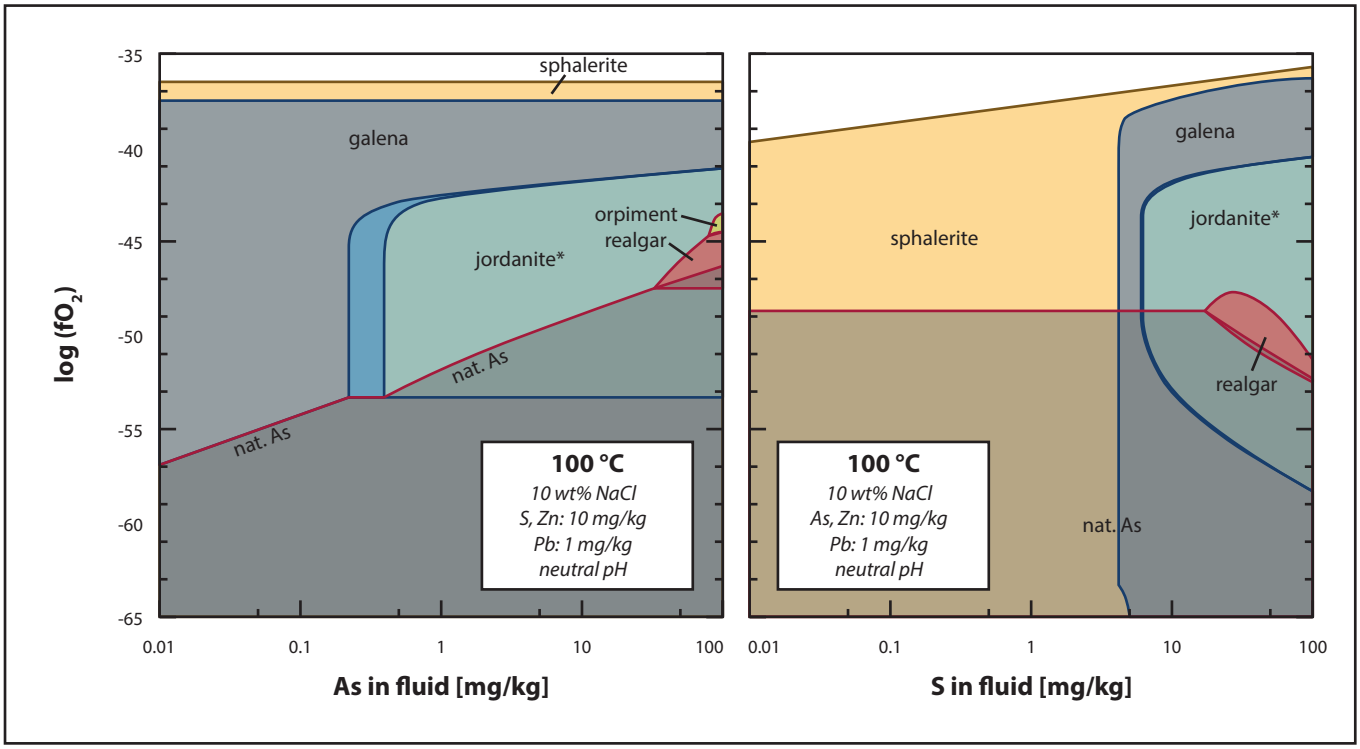
-35
-40
-45
-50
-55
-60
-65
log (fO2)
sphalerite
galena
orpiment
realgar
jordanite*
nat. As
nat. As
100 °C
10 wt% NaCl
S, Zn: 10 mg/kg
Pb: 1 mg/kg
neutral pH
0.01
0.1
1
10
100
As in fluid [mg/kg]
sphalerite
galena
jordanite*
realgar
nat. As
100 °C
10 wt% NaCl
As, Zn: 10 mg/kg
Pb: 1 mg/kg
neutral pH
0.01
0.1
1
10
100
S in fluid [mg/kg]

Figure 12

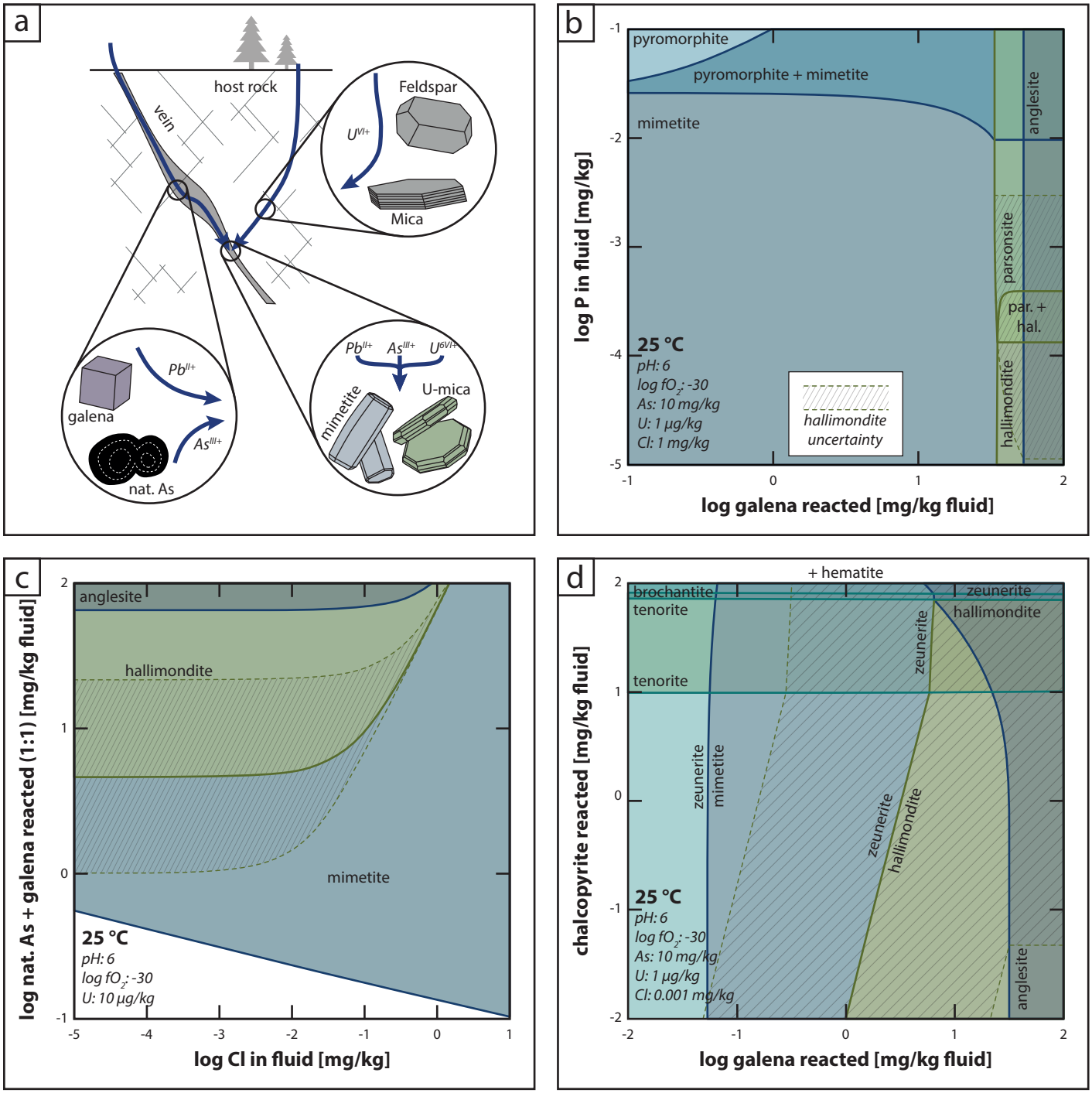
a
host rock
vein
Feldspar
U^{VI+}
Mica
galena
Pb^{II+}
As^{III+}
nat. As
Pb^{II+} As^{III+} U^{6VI+}
U-mica
mimetite
b
pyromorphite
pyromorphite + mimetite
mimetite
anglesite
parsonsite
par. + hal.
hallimondite
25 °C
pH: 6
log fO_2: -30
As: 10 mg/kg
U: 1 µg/kg
Cl: 1 mg/kg
hallimondite uncertainty
log P in fluid [mg/kg]
log galena reacted [mg/kg fluid]
c
anglesite
hallimondite
mimetite
25 °C
pH: 6
log fO_2: -30
U: 10 µg/kg
log nat. As + galena reacted (1:1) [mg/kg fluid]
log Cl in fluid [mg/kg]
d
+ hematite
brochantite
tenorite
tenorite
zeunerite
hallimondite
zeunerite
zeunerite
mimetite
zeunerite
hallimondite
anglesite
25 °C
pH: 6
log fO_2: -30
As: 10 mg/kg
U: 1 µg/kg
Cl: 0.001 mg/kg
chalcopyrite reacted [mg/kg fluid]
log galena reacted [mg/kg fluid]